J. metamorphic Geol., 2007, **25,** 187–206 doi:10.1111/j.1525-1314.2006.00688.x

Petrogenesis of the garnet peridotite and garnet-free peridotite of the Zhimafang ultramafic body in the Sulu ultrahigh-pressure metamorphic belt, eastern China

J. S YANG,[1] R. Y. ZHANG,[2] T. F. LI,[1] Zh. M. ZHANG[1] AND J. G. LIOU[2]
[1]*Key Laboratory for Continental Dynamics, Institute of Geology, Chinese Academy of Geological Sciences, 26 Baiwanzhuang Road, Beijing, 100037, China (yangjsui@ccsd.cn)*
[2]*Department of Geological and Environmental Sciences, Stanford University, Stanford, CA 94305, USA*

ABSTRACT The CCSD-PP1 drillhole penetrated a 110-m-thick sequence of the Zhimafang ultramafic body in the Sulu ultrahigh-pressure (UHP) metamorphic belt, east China. The sequence consists of interlayered garnet-bearing (Grt) and garnet-free (GF) peridotite. Eleven layers of Grt-peridotite, ranging from 1.2 to 9.5 m in thickness, have an aggregate thickness of 54.49 m, whereas eight layers of GF-peridotite, ranging from 2.2 to 14.2 m in thickness, have a total thickness of 57.53 m. The boundaries between the two rock types are gradational. The Grt-peridotites have slightly higher contents of Al_2O_3, CaO and SiO_2, and lower $Mg^{\#}$s (0.90–0.92) than the GF-peridotites ($Mg^{\#}$s 0.91–0.93). Both contain low TiO_2 (< 0.05 wt%) and have higher modal abundances of enstatite (average 10 vol.%) than diopside (1–5 vol.%), typical of depleted-type upper mantle. The diopside in these rocks has high and relatively uniform $Mg^{\#}$ members (0.93–0.95), but highly variable Al_2O_3 (0.2–2.3 wt%), Na_2O (0.5–2.5 wt%) and Cr_2O_3 (0.38–2.09 wt%). Enstatite (En_{92-93}) contains very low Al_2O_3 (0–0.3 wt%). Both porphyroblastic and equigranular garnet are present. The equigranular varieties are zoned, from core to rim in Cr_2O_3 (3.4–4.2 wt%), MgO (18.4–17.5 wt%) and Al_2O_3 (21.1–20.1 wt%). Titania is very low in all the garnet, mostly < 0.05 wt%. Chromite or chromium (Cr)-spinel occur both in the Grt- and GF-peridotite, and are characterized by high contents of Cr_2O_3 (49–58 wt%) and FeO (24–43 wt%), similar to that in iron-rich Alpine-type peridotites. Based on the bulk-rock MgO–FeO compositions, the Zhimafang Grt-peridotite probably underwent 20–30% partial melting, whereas the GF-peridotite may have undergone as much as 35–40% partial melting, suggesting that the two rock types owe their differences to different degrees of partial melting rather than to pressure differences during metamorphism.

Key words: CCSD-PP1; garnet peridotite; mantle; Sulu; UHP.

INTRODUCTION

Since the discovery of coesite in the Dabie Mountains (Xu, 1987; Okay *et al.*, 1989; Wang *et al.*, 1989; Hirajima *et al.*, 1990), the Dabie-Sulu terrane has been recognized as the largest well-preserved, ultrahigh-pressure metamorphic (UHPM) belt in the world (Jahn, 1998; Liou & Zhang, 1998). This belt formed at *c.* 220 Ma by convergence of the Yangtze Block to the south and North China Block to the north (Ames *et al.*, 1993; Li *et al.*, 1993; Hacker & Wang, 1995). Numerous geochemical and isotopic studies of the UHPM rocks in the belt, coupled with structural and geophysical investigations, have provided a better understanding of the processes of continental subduction, collision and exhumation at convergent plate boundaries (e.g. Cong *et al.*, 1992; Zhang & Liou, 1994). Stable isotope geochemistry provides unequivocal evidence that the protoliths of the UHPM eclogites and gneisses were at the surface prior to continental collision and subduction (Rumble & Yui, 1998). The recent discovery of diamonds in the ultramafic rocks and eclogites at Donghai, south of the Sulu region, confirms that the UHPM rocks were subducted to greater depths than those of most other UHPM belts (Yang *et al.*, 1999; Xu *et al.*, 2005).

After more than 10 years of study, the Dabie-Sulu UHPM belt was selected by the International Continental Scientific Drilling Program as an appropriate location for deep drilling, which was carried out by the Chinese Continental Scientific Drilling Project (CCSD) (Xu *et al.*, 1998). One of the main goals of the drilling was to study the behaviour of mantle rocks in a subduction zone and to understand better the mechanisms of subduction and exhumation of these rocks.

Many ultramafic blocks, ranging in size from a few tens of metres to kilometres, occur in the Dabie-Sulu UHPM belt. They are generally believed to represent mantle rocks, which were first emplaced into the upper crust and then subducted during continental collision, and finally exposed to the surface during exhumation or by subsequent geological events (Yang, 1991; Zhang *et al.*, 1994; Liou & Zhang, 1998). An alternative interpretation is that they are fragments of a mantle

© 2007 Blackwell Publishing Ltd

wedge, which were carried into the deep mantle during subduction and then exhumed along with the subducted continental crust (Zhang *et al.*, 2000). However, very little information is available for these rocks because they occur in small, isolated outcrops and are typically highly weathered. The CCSD drilled a number of holes in the Sulu UHP belt, which recovered several continuous sections of fresh ultramafic rock. We investigated these rocks to determine their original textures and compositions, their behaviour during UHP metamorphism and the processes by which they were exhumed and emplaced. In this study, the results of petrological investigation of continuous peridotite core samples recovered from the pre-pilot hole PP1 of the CCSD project are presented.

GEOLOGY OF THE ZHIMAFANG PERIDOTITE MASSIF

The Qinling-Dabie-Sulu orogenic belt – which extends for over 1000 km across east-central China east–west and is ~200 km wide – separates the Yangtze craton on the south from the Sino-Korean craton on the north (see insert in Fig. 1). The Tanlu fault cuts the belt into two parts, the Dabie sub-belt in the west and the Sulu sub-belt in the east. Each sub-belt includes three tectonic units: a northern high-grade metamorphic complex, a central UHP unit and a southern high-pressure (HP) unit (Xu *et al.*, 1998). The Donghai area (Donghai here is a county name) is located in the central UHP unit of the Sulu sub-belt (Fig. 1a).

Although dozens of ultramafic blocks are exposed in the Donghai area, they have not been systematically studied because of poor exposure and intense weathering. The Zhimafang ultramafic massif is a relatively large block located ~30 km east of Donghai county, Jiangsu province. The massif occurs as a lens, ~1000 m long, 60–180 m wide and 50–100 m thick, hosted in gneiss (Fig. 1b). Core recovered from the CCSD pre-pilot hole (CCSD-PP1), and several other previous drill holes, provides an extraordinary opportunity for studying a continuous section of a garnet peridotite massif.

The ultramafic blocks commonly have sharp tectonic contacts with their country rocks, which consist mainly of granitic gneiss, with lesser amounts of other gneiss, jadeite quartzite and marble. Large volumes of the gneissic rocks in this belt have been shown to have undergone UHP metamorphism (Wang & Liou, 1991; Okay & Sengor, 1992; Liu *et al.*, 2002, 2004). The ultramafic rocks differ significantly in lithology and occurrence in the region, but there are two dominant types: one consists solely of ultramafic rock, and the other is a complex containing both mafic and ultramafic material. The main rock types are harzburgite, lherzolite, wehrlite and pyroxenite. Garnet and phlogopite are very common in the ultramafic rocks, but both Grt- and GF-peridotites are present.

The CCSD-PP1 drillhole penetrated to a total depth of 432 m with a core recovery of over 80%. Lithologically, the core can be divided into three parts: upper gneisses, middle ultramafic rocks and lower gneisses (Fig. 1c). The upper sequence consists mainly of hornblende-plagioclase gneiss, hornblende-monzonitic gneiss and biotite-plagioclase gneiss, whereas the lower unit is a 180-m-thick sequence of granitic gneiss. A 3-m-thick lens of eclogite occurs in the upper gneiss and a 5-m-thick eclogite layer is hosted in the lower gneiss, and both of them have transitional contacts with their host rocks. There are also several thin (0.5–1 m) layers of schist in the gneisses, and the contacts between the two are concordant. These rocks consist mainly of phengite quartz schist and epidote hornblende schist, although kyanite is also common.

The middle ultramafic section, which includes a 7-m-thick layer of gneiss, is 118.55 m thick and lies between depths of 137.82 and 256.37 m (Fig. 2). The core provides a nearly continuous sequence of the ultramafic rock, and preserves the boundaries between the different lithological units. A shear zone separates the ultramafic rocks from the upper gneisses, and the adjacent rocks are highly sheared and altered. Along the contact, the ultramafic rocks are intensely serpentinized but they become fresher towards the interior of the block (Figs 1d & 3). The ultramafic rocks host a 5-m-thick layer of gneiss and a 2-m-thick phlogopite vein near their lower boundary. At the top, the lower contact with the underlying gneiss is a shear zone, although the contact has been obscured during or after emplacement of the block.

The ultramafic rocks are subdivided into Grt-peridotite (mineral symbols after Kretz, 1983) and GF-peridotite. The two different types form intercalated layers, separated by gradational contacts. Eleven layers of Grt-peridotite, ranging in thickness from 1.2 to 9.5 m have an aggregate thickness of 54.49 m, whereas eight layers of GF-peridotite (2.2–14.2 m thick) total 57.53 m. The rocks are only weakly serpentinized, and the transitional boundaries between the Grt- and GF-peridotite are well preserved. The transition from one variety to another typically takes place over a few centimetres. Data on specific layers are given in Table 1.

LITHOLOGY

Several varieties of Grt-peridotite and GF-peridotite are recognized based on their mineralogy, particularly the relative abundance of clinopyroxene and orthopyroxene. In this study, the nomenclature of Streckeisen (1976) is used. Rocks containing >90% serpentine are termed 'serpentinite'.

Garnet peridotite

Garnet peridotites include garnet harzburgite and lherzolite, and consist of variable amounts of olivine, enstatite, diopside, garnet and phlogopite. Small

© 2007 Blackwell Publishing Ltd

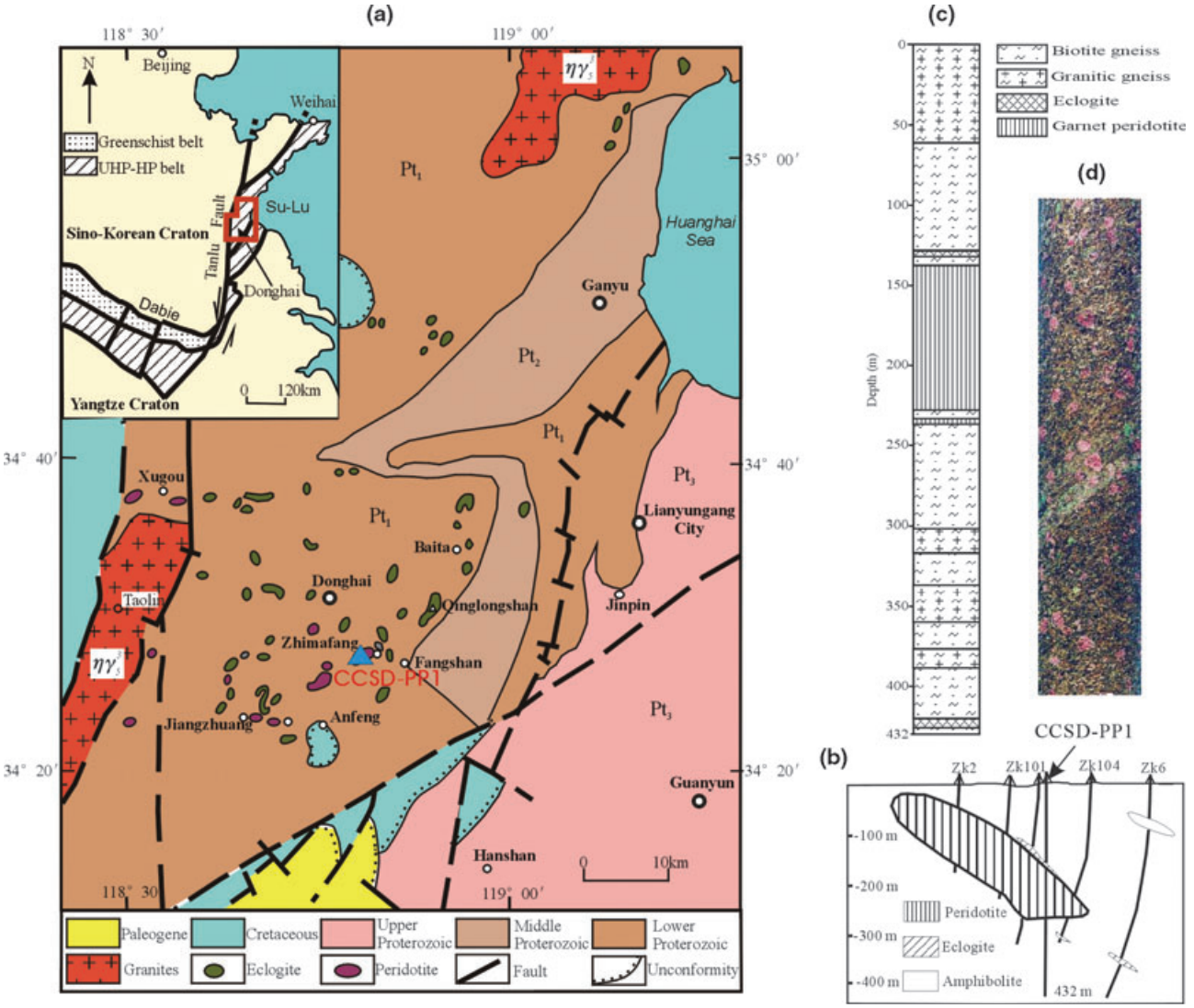


Fig. 1. (a) Simplified geological map of the southern Sulu region. (b) Profile of the Zhimafang ultramafic body and location of the PP1 drillhole of the Chinese Continental Scientific Drilling (CCSD). (c) Simplified column of the main lithological units of the PP1. (d) Photograph of the garnet peridotite core.

amounts of titanoclinohumite (Ti-Chu), chromite, carbonate and apatite occur in some layers. The rocks are variably foliated and minerals, especially phlogopite, are clearly oriented, but the degree of deformation varies in different rocks. Garnet lherzolite and harzburgite usually have porphyroblastic, equigranular and mosaic textures, with typical triple-junction (120°) grain boundaries (Fig. 3a). The rocks consist of 5–15 vol.% garnet, 70–80% olivine, 5–8% orthopyroxene, 1–3% clinopyroxene, 3–5% of phlogopite and 1–2% chromite.

Porphyroblastic garnet forms crystals up to 20 mm in diameter, although most are <10 mm. The garnet crystals are set in a relatively fine-grained (<2 mm) matrix of olivine (Ol), enstatite (En), diopside (Di), garnet (Grt) and phlogopite (Phl) (Fig. 3b). Individual crystals are commonly subhedral with curved or irregular boundaries. Many contain mineral inclusions, such as olivine and orthopyroxene or their alteration products, suggesting that these porphyroblasts grew later than the matrix minerals (Fig. 3b). The porphyroblastic garnet is rimmed by amphibole + Cr-spinel (or Cr-rich magnetite), with or without phlogopite, and some grains are totally replaced by chlorite ± calcite or by chlorite, mica and opaque dust (Cr-magnetite).

Small grains of garnet (~1 mm) are also common in the groundmass, mostly euhedral to rounded, and scattered throughout the rock. An important phenomenon is that small garnet, even very small ones, are always spatially associated with enstatite (Fig. 3a,c). Like the porphyroblasts, the groundmass garnet contains inclusions of enstatite, olivine and chromite (Fig. 3c).

Olivine, ~1–2 mm in size, has an equilibrium texture with co-existing enstatite and, sometimes with

© 2007 Blackwell Publishing Ltd

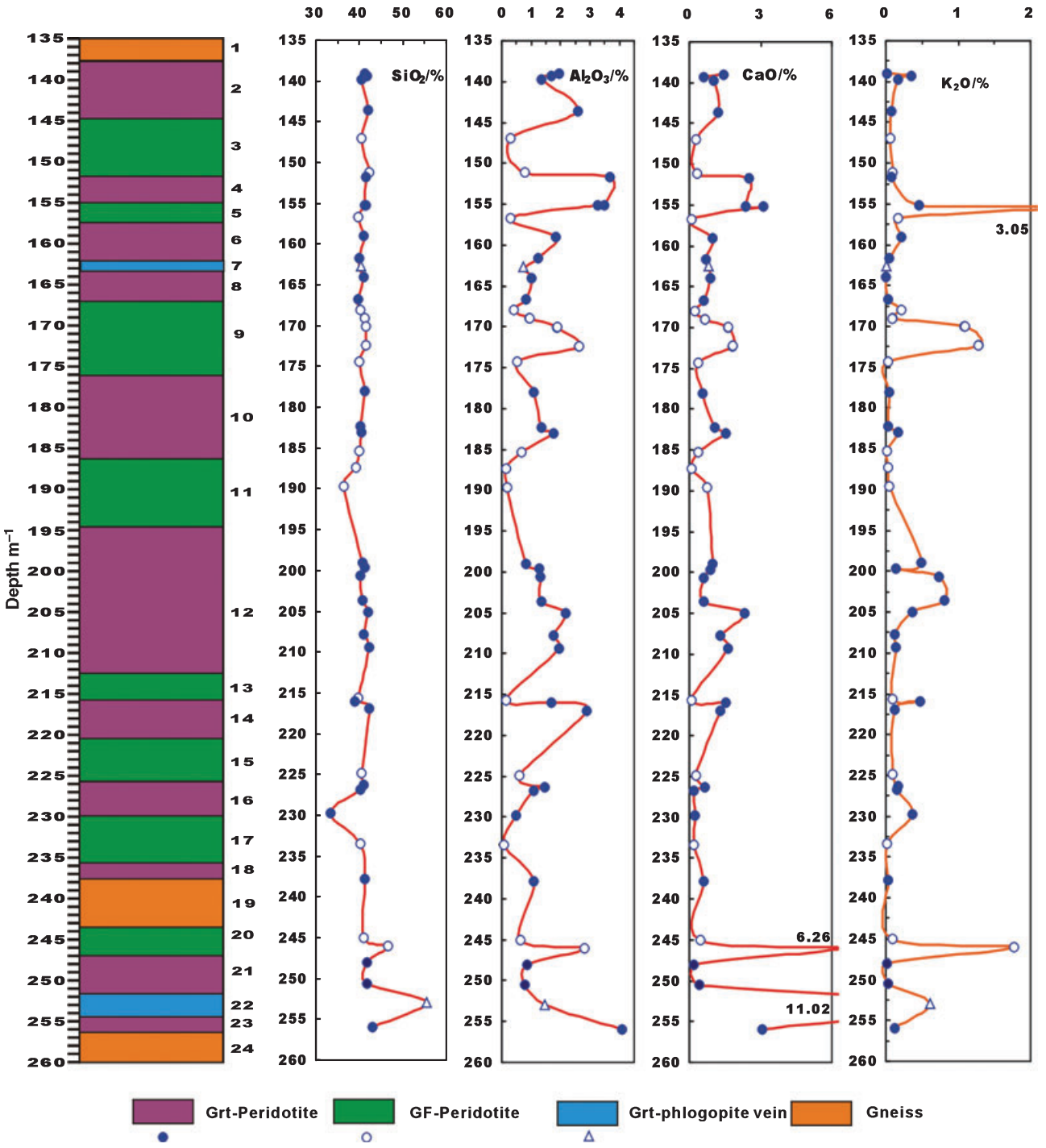


Fig. 2. Column of the ultramafic section in the PP1 drillhole, 24 lithological units are recognized, including 11 units of Grt-peridotite and eight units of Gf-peridotite. For detailed information on each unit see Table 1; CaO and Al_2O_3 contents in compositional profiles show a consistent variation with rock type, but K_2O shows an irregular variation.

groundmass garnet. It typically contains a few very small exsolved ilmenite lamellae, and inclusions of olivine may occur in the garnet.

Enstatite and diopside range from 0.3 to 1.5 mm in diameter, but most grains are < 1 mm in size. Diopside is light green in fresh samples, but is replaced by tremolite and chromite in zones of retrograde metamorphism and in metasomatic domains. Exsolved lamellae of titanoclinochumite, titanochondrodite (Xu *et al.*, 2003) and phlogopite commonly occur in

© 2007 Blackwell Publishing Ltd

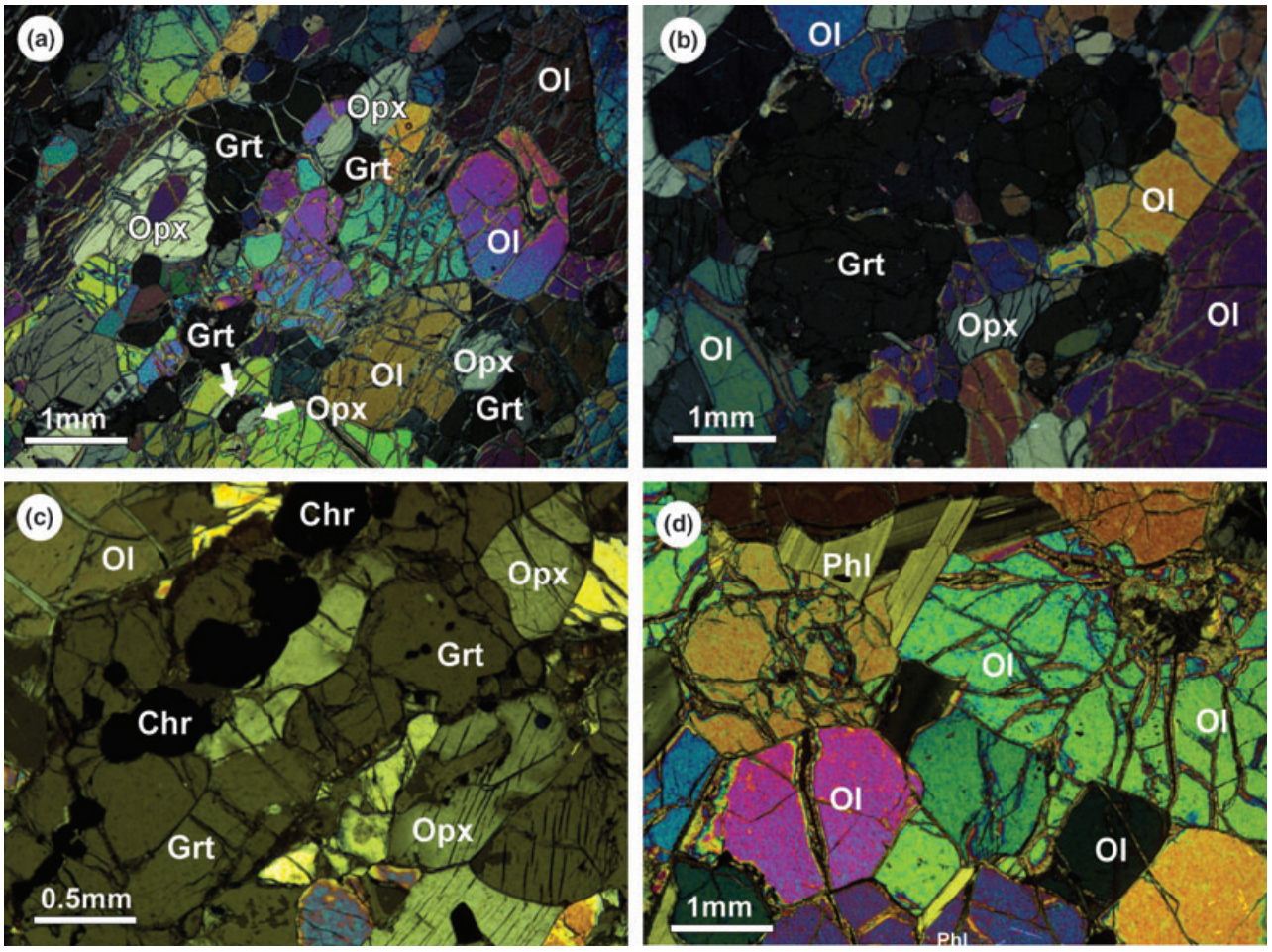


Fig. 3. Microphotographs of garnet peridotite and garnet-free peridotite. (a) Grt-harzburgite c21-134-55): equigranular structure, garnet spatially associated with Opx, even very small one (see arrow). (b) Grt-harzburgite (c34-151-74): porphyroblastic garnet with olivine inclusions. (c) Grt-harzburgite (c25-141-60): spatial association of garnet, Opx and chromite. (d) Dunite (c31-147-68): equigranular structure without deformation.

diopside. Enstatite may be completely fresh or partly replaced by talc. A few enstatite grains contain exsolved lamellae of diopside and chromite.

Phlogopite occurs as small flakes ~0.1–0.2 by 0.5–1 mm in size. Minute grains of titanoclinohumite (0.1–0.2 mm) are locally included in olivine and pyroxene crystals, and minor aggregates of magnesite or dolomite occur in the matrix. Very small crystals of chromite are present as inclusions in garnet and in the matrix. A few relatively large grains of diopside, commonly with exsolution lamellae of enstatite, are also present.

In general, harzburgites, wehrlites and dunites are similar to the garnet lherzolite in texture, but differ from lherzolite in mineral proportions. The harzburgites contain <5 vol.% diopside and dunite is composed of olivine and minor ($<10\%$) phlogopite, garnet and pyroxene. In some foliated harzburgites and lherzolites all the minerals, including olivine, diopside, enstatite and phlogopite, are elongated with length/width ratios of 2:1 to 6:1 and well oriented.

Garnet-free peridotite

Garnet-free peridotite includes harzburgite, dunite and wehrlite, all of which have relatively high and variable amounts of chromite. The rocks are mainly characterized by typical equigranular, less foliated textures, an absence of porphyroblasts, and weak serpentinization. They consist of 80–90 vol.% olivine, 10–20% orthopyroxene, 1–3% clinopyroxene, 3–5% phlogopite and 2–3% chromite. Olivine grains are ~1–2 mm in size, and show typical triple-junction (120°) grain boundaries (Fig. 3d).

The harzburgites have an average of 10 vol.% orthopyroxene and 1–3 vol.% diopside. Orthopyroxene occurs both as large crystals in equilibrium with coarse-grained olivine, and as small interstitial grains typically associated with small olivine and diopside. Most of the diopside forms small, interstitial grains but a few large crystals with exsolution lamellae of enstatite are also present. No diopside exsolution lamellae

© 2007 Blackwell Publishing Ltd

Table 1. Lithological units in the PP1 drillhole

Unit no.	Rock name	Sample no.	Depth	Unit depth	Unit thickness	Sample brief description
1. Country rocks						
	Gneiss	C20-129-51	137.82			
	Mafic rock	C20-130-52	138.50	138.75		
2. Grt-peridotite						
	Grt-Harzburgite	C21-132-53	139.00		6.54	80% serp, Fo 91, opx 10% En 92, cpx few, phlog few
	Grt-Harzburgite	C21-133-54	139.30			grt + sp, highly serp, Fo 91, sp few
	Grt-Harzburgite	C21-134-55	139.75			40% serp, grt small, Fo 92,opx 30%, phlog <5%
	Grt-Lherzolite	C22-135-56	143.57	145.29		grt + sp, 50% serp, grt 10%, cpx few, sp few
3. GF-peridotite						
	Harzburgite	C23-136-57	147.00		6.15	highly serp, phlog few
	Harzburgite	C23-139-58	151.14	151.44		highly serp, Fo 92
4. Grt-peridotite						
	Grt-Harzburgite	C24-141-59	151.74		3.58	grt + sp, 50% serp, Fo 92, En 92, sp in grt, phlog
	Grt-Harzburgite	C25-141-60	155.16			fresh, Fo 93, opx 20% En 92, grt small 20%
	Grt-Harzburgite	C25-143-61	155.16	155.02		grt + sp, fresh, Fo 91, opx 30% En 92, sp in grt, grt small & large, phlog
5. GF-peridotite						
	Dunite	C26-143-62	156.68	157.84	2.82	fresh, ol 1–3 mm, sp 2%, phlog 5%
6. Grt-peridotite						
	Grt-Harzburgite	C27-144-63	159.00		9.49	fresh, corsed and fine gain layers, Fo 93, En 95
	Grt-Harzburgite	C27-144-64	161.65	162.3		
7. Grt-peridotite						
	Grt-Phlog vein	C28-145-65	162.95	163.52	1.22	large grt >2 cm, small grt 1-2 mm, phlog 2-3 mm
8. Grt-peridotite						
	Grt-Harzburgite	C30-146-66	164.00		3.83	highly serp, grt few, En 96
	Grt-Harzburgite	C30-146-67	166.65	167.35		fresh,small grt 5%, Fo 92, opx few En 93
9. GF-peridotite						
	Dunite	C31-147-68	168.00		8.8	fresh, large ol 3–5 mm, samll ol < 1 mm, opx 3%, phlog 2%
	Lherzolite	C31-148-69	169.00			fresh, Fo 92, phlog 5%, 2–4 mm or <1 mm
	Lherzolite	C31-149-70	170.05			fresh, Fo 92, cpx 20%, phlog 5%, sp 2%
	Lherzolite	C32-149-71	172.37			foliated, Fo 91, phlog 20% oriented
	Harzburgite	C33-150-72	174.30	176.15		fresh, Fo 89, opx 10% zoning, sp 2%, phlog few, dol
10. Grt-peridotite						
	Grt-Harzburgite	C34-150-73	178.00		9	grt + sp, fresh foliated, Fo 92, grt few, opx 15% En 93, sp in grt, phlog 15%
	Grt-Harzburgite	C34-151-74	182.27			fresh foliated, Fo 92, grt 1–2 mm or <0.5 mm, En 93, phlog 5% oriented
	Grt-Harzburgite	C35-152-75	183.00	185.15		Fo 93, En 93
11. GF-peridotite						
	Lherzolite	C35-153-76	185.30		14.15	50% serp, ol corsed grain,Fo 92, amph after cpx
	Dunite	C36-153-77	187.30			fresh, zoning, Fo 93, opx 10%, sp 2% XCr 0.90, XMg 0.21,magn, phlog few
	Harzburgite	C37-154-78	189.60			50% serp,opx 15%, serp & mgs zonig, mgs, phlog 5%
	Harzburgite	C38-156-79	199.00	199.3		fresh, foliated,1–2 mm or <1 mm zoning, Fo 92, opx 15%, phlog <10%
12. Grt-peridotite						
	Grt-Harzburgite	C38-157-80	199.60		2.6	grt + sp, 40% serp,Fo 92, opx 10% En 96, sp few, phlog few
	Grt-Harzburgite	C39-157-81	200.60	202.1		grt + sp, grt 20% phlog after grt, Fo 91, Sp XMg 0.12, XCr 0.99, phlog
13. GF-peridotite						
	Harzburgite	C40-158-82	203.60	204.3	2.2	fresh, foliated,ol 7–8 mm or 1 mm, Fo 93, opx 1 mm En 95, phlog 10%
14. Grt-peridotite						
	Grt-Harzburgite	C41-159-83	205.00		7.9	50% serp, Fo 90, opx 10% En 92, phlog 10%
	Grt-Harzburgite	C42-159-84	207.75			
	Grt-Harzburgite	C43-160-85	209.35	212.2		50% serp, chl after grt, Fo 92, En 94
15. GF-peridotite						
	Dunite	C45-163-86	215.64		13.36	50% serp, coarsed ol, Fo 93, opx <5%
	Lherzolite	C46-164-87	216.00			50% serp, foliated,ol coarsed grain, opx 5%, sp 3%, gagn & phlog vein, phlog 10%
	Lherzolite	C46-164-89	216.94			Fo 92, En 94, Sp XMg 0.22, XCr 0.95
	Harzburgite	C47-165-90	224.86	225.56		slight serp, ol 1-2 mm Fo 93, opx <10% En 93, sp few, phlog 2–3%
16. Grt-peridotite						
	Grt-Harzburgite	C48-166-91	226.27		2.71	slight serp, grt 1 mm or <0.5 mm, Fo 92.6, En 96, phlog 5%
	Grt-Harzburgite	C49-166-92	226.77	228.27		Fo 90, En 93, Mgs, phlog, Ti-Chu
17. GF-peridotite						
	Harzburgite	C50-166-93	229.77		7.33	fresh,ol coarsed grain, Fo 88, opx 5%, sp 3%, phlog 5%
	Harzburgite	C51-167-94	233.40	235.6		fresh, ol 90%, coarsed, Fo 93 or 89, opx < 10%, En 92.1, few Sp XMg 0.24, XCr 0.95, talc
18. Grt-peridotite						
	Grt-Harzburgite	C52-169-95	237.81	238.16	2.56	highly serp, Fo 92, En 92, sp XMg 0.35 XCr 0.87
19. Gneiss				243.5	7.9	
20. GF-peridotite						
	Harzburgite	C55-172-98	245.00		3.5	highly serp, Fo 92, phlog
	Harzburgite	C55-173-99	246.00	247		highly serp, folicated, Fo 90, phlog + mgs 50%, sp 3%
21. Grt-peridotite						
	Grt-Harzburgite	C55-175-100	248.00		4.78	50% serp, Fo 91, chl after grt
	Grt-Harzburgite	C55-176-101	250.56	251.78		50% serp
22. GF-peridotite						
	Phlogopite vein	C56-176-102	253.00	254.5	2.72	phlog 80%, foliated, amph 10–20%, mgt locally concentrated
23. Grt-peridotite						
	Grt-Harzburgite	C56-177-103	256.00	256	1.5	highly serp, ol 20% relic, 1 cm, Fo 89, chl after grt
24. Gneiss						

Grt-peridotite: total 11 units and 54.49 m, single unit thickness 1.2-9.5 m.
GF-peridotite: total eight units and 57.53 m, single unit thickness 2.2-14.2 m.

© 2007 Blackwell Publishing Ltd

have been observed in the enstatite crystals. Small grains of phlogopite are in equilibrium with other minerals, whereas the large grains (up to 10 mm across) commonly crosscut other minerals or occur as phenocrysts. Small grains of chromite (< 0.5 mm) are euhedral and ubiquitous either as interstitial material or as inclusions in olivine and orthopyroxene.

Fresh dunite consists of > 90 vol.% olivine, ~5% phlogopite and ~3% chromite, and has an equigranular texture. Olivine and phlogopite range from 1.3 to 4 mm in diameter, whereas chromite is fine-grained (0.1–0.6 mm). The chromite occurs both as inclusions in olivine and as interstitial grains.

Ti-clinohumite-bearing peridotite

Most of the Ti-clinohumite in the Zhimafang peridotites occurs as inclusions in olivine and pyroxene, but some large crystals are also present. In addition, minor Ti-Chu occurs in a vein composed mainly of Mgs + Phl.

CHEMICAL COMPOSITIONS

Major- and trace-element analyses of 25 samples of Grt-peridotite and 16 samples of GF-peridotite were carried out at the National Geological Analysis Center, Beijing, China and discussed by Li *et al*. (unpubl. data). Ten representative analyses are listed in Table 2.

Both Grt-peridotite and GF-peridotite are magnesium-rich ultramafic rocks with similar $Mg^{\#}$ [Mg/(Mg + Fe)] (mostly 0.90–0.92). They exhibit regular variations in bulk-rock compositions, particularly in the concentrations of Al_2O_3, CaO, SiO_2 and MgO (Fig. 4). Alumina, CaO and SiO_2 in both varieties correlate negatively with MgO + FeO* (MgO wt% plus total FeO wt%). Cr_2O_3, NiO and FeO* vary over a small range, but K_2O shows wide and random variations.

Table 2. Representative compositions of garnet and garnet-free peridotite in PP1 drillcore

Sample:	C26-143-62	C31-147-68	C35-153-76	C36-153-77	C51-167-94	C27-144-64	C35-152-75	C38-157-80	C42-159-84	C48-166-91
Depth:	156.68	168.00	185.30	187.30	233.40	161.65	183.00	199.60	207.75	226.27
Rock:	GF-perid.	GF-perid.	GF-perid.	GF-perid.	GF-perid.	Ga-perid.	Ga-perid.	Ga-perid.	Ga-perid.	Ga-perid.
SiO_2	41.32	41.87	41.48	41.05	41.58	42.21	41.31	42.44	42.41	42.78
TiO_2	0.01	0.01	0.00	0.01	0.00	0.02	0.01	0.00	0.01	0.01
Al_2O_3	0.30	0.42	0.72	0.17	0.07	1.31	1.80	1.32	1.82	1.53
Cr_2O_3	0.51	0.23	0.41	0.46	0.31	0.47	0.38	0.53	0.36	0.44
TFe_2O_3	8.10	7.65	8.21	8.29	7.41	8.14	7.99	7.32	7.84	7.59
FeO	6.27	6.40	6.74	6.79	6.05	7.26	6.11	5.80	6.64	6.54
MnO	0.12	0.10	0.12	0.12	0.10	0.12	0.12	0.11	0.12	0.11
MgO	47.02	47.08	45.63	47.44	47.18	45.00	42.25	43.92	42.51	44.13
CaO	0.11	0.23	0.41	0.12	0.18	0.73	1.57	0.89	1.35	0.67
Na_2O	0.02	0.02	0.03	0.02	0.16	0.11	0.09	0.07	0.09	0.06
K_2O	0.18	0.22	0.02	0.04	0.02	0.06	0.17	0.14	0.12	0.18
P_2O_5	0.10	0.10	0.10	0.10	0.10	0.10	0.10	0.10	0.10	0.10
NiO	0.28	0.28	0.27	0.29	0.31	0.24	0.25	0.24	0.23	0.26
LOI	2.74	1.51	2.67	2.60	2.96	1.90	4.70	3.20	3.72	2.72
Total	100.70	99.61	99.98	100.60	100.33	100.30	100.64	100.18	100.58	100.48
FeO*	7.49	7.07	7.65	7.67	6.90	7.51	7.55	6.84	7.34	7.04
MgO + FeO*	55.78	55.36	54.85	56.40	55.67	53.56	51.85	52.38	51.51	52.47
$Mg^{\#}$ (ppm)	0.92	0.92	0.92	0.92	0.93	0.92	0.91	0.92	0.91	0.92
La	7.010	0.500	3.010	2.190	1.890	10.600	3.830	3.800	3.870	12.800
Ce	12.800	1.190	6.270	5.100	5.200	17.400	8.600	10.800	9.800	27.900
Pr	1.620	0.130	0.570	0.490	0.400	2.080	1.320	0.860	0.820	2.240
Nd	6.210	0.540	2.020	1.960	1.530	7.530	3.060	3.420	3.000	7.780
Sm	1.160	0.150	0.370	0.420	0.330	1.520	0.540	0.720	0.580	1.510
Eu	0.340	0.070	0.130	0.170	0.160	0.370	0.190	0.230	0.180	0.470
Gd	1.130	0.200	0.380	0.350	0.330	0.740	0.540	0.590	0.490	0.850
Tb	0.220	0.060	0.062	0.053	0.055	0.240	0.090	0.088	0.072	0.210
Dy	1.040	0.160	0.320	0.250	0.260	1.220	0.510	0.420	0.360	1.040
Ho	0.240	0.040	0.079	0.059	0.063	0.290	0.130	0.099	0.092	0.240
Er	0.430	0.060	0.140	0.110	0.110	0.530	0.270	0.190	0.180	0.420
Tm	0.080	0.010	0.026	0.019	0.020	0.091	0.050	0.033	0.033	0.070
Yb	0.520	0.120	0.180	0.130	0.140	0.600	0.330	0.230	0.220	0.460
Lu	0.070	0.010	0.030	0.022	0.027	0.092	0.058	0.038	0.038	0.072
Rb	5.340	5.720	1.500	1.260	3.640	2.080	4.710	4.060	3.800	5.770
Ba	130.000	85.900	53.100	58.100	119.000	109.000	152.000	166.000	171.000	267.000
Sr	18.200	15.700	16.700	5.300	33.500	25.300	52.500	54.900	41.200	58.400
Th	0.640	0.200	0.420	0.840	0.190	0.580	0.840	1.820	1.000	2.520
U	0.190	0.090	0.160	0.140	0.043	0.062	0.130	0.150	0.064	0.230
Nb	0.300	0.400	1.660	4.000	0.760	0.370	1.460	1.060	1.390	1.180
Ta	0.003	0.004	0.280	0.260	0.068	0.140	0.300	0.160	1.040	0.410
Zr	9.200	20.100	1.030	0.580	3.730	0.860	1.160	0.950	1.830	3.380
Hf	0.023	0.000	0.045	0.032	0.015	0.036	0.075	0.087	0.090	0.120
Y	4.780	0.830	1.740	1.330	1.370	6.700	3.180	2.190	2.170	5.300
Sc	4.000	8.500	10.300	10.800	6.700	11.100	15.600	16.800	16.900	9.130
V	21.300	17.100	16.400	9.100	20.500	27.100	32.100	23.200	26.500	19.200
Co	57.500	62.000	103.000	103.000	171.000	110.000	107.000	95.100	94.300	91.000

© 2007 Blackwell Publishing Ltd

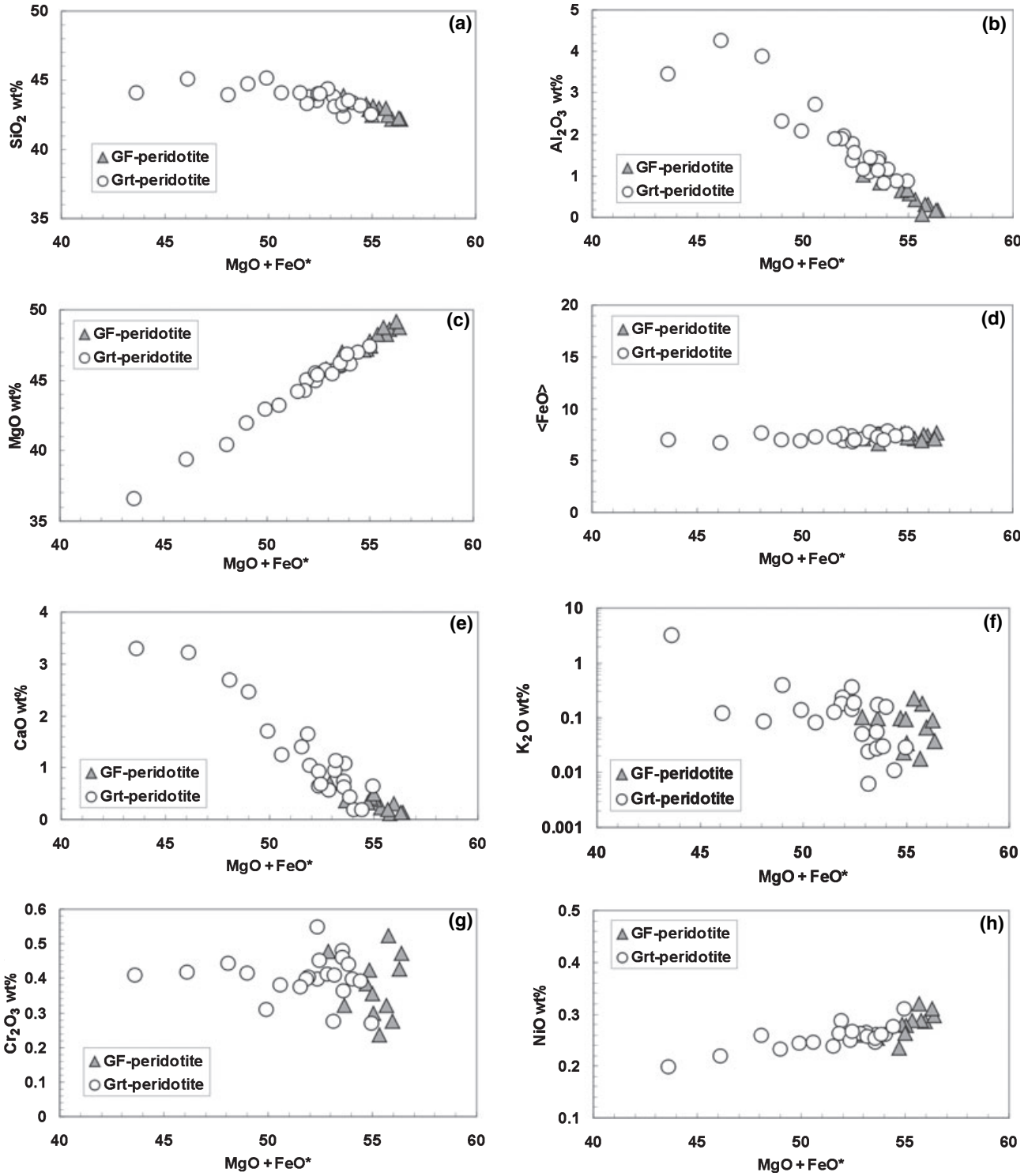


Fig. 4. SiO_2, MgO, FeO*, Al_2O_3, CaO, K_2O, Cr_2O_3, Na_2O, Al_2O_3 and NiO *v.* MgO + FeO* diagrams (a–h). The Grt-peridotite is easily distinguished from the GF-peridotite by higher Al_2O_3, CaO and SiO_2, and lower MgO and NiO, and similar contents of Cr_2O_3 and K_2O.

Although the two type rocks overlap in composition (Fig. 4), the Grt-peridotites have somewhat higher contents of Al_2O_3 (most >1 wt%), CaO (most 0.6–1.6 wt%) and SiO_2, and lower MgO (40–45 wt%) than the GF-peridotites. In addition, the Grt-peridotites have much higher abundances of Sc, Ba, Sr and V than

© 2007 Blackwell Publishing Ltd

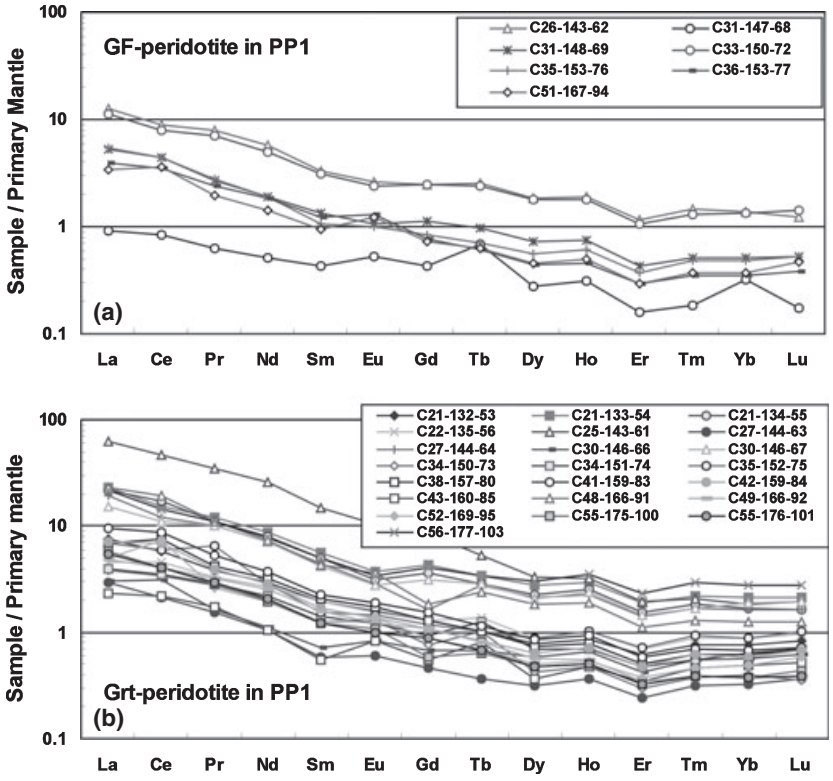


Fig. 5. REE chrondite-normalized patterns for GF-peridotite and Grt-peridotite showing LREE-enriched chondrite-normalized patterns, with the REE abundances of the Grt-peridotite being higher than those of the GF-peridotite.

the GF-peridotites, although both have similar abundances of Cr, Ni and Ti. The $Mg^{\#}$s of the Grt-peridotites (0.90–0.92) are slightly lower than those of the GF-peridotite (0.91–0.93), but both belong to the depleted-type upper mantle.

Both the Grt-peridotite and GF-peridotite have similar chondrite-normalized REE patterns showing slight enrichment in LREE (Fig. 5). The $[La/Yb]_N$ ratios for the GF-peridotites range from 2.8 to 8.9 (average 7.0) and are very similar to those of the Grt-peridotite (2.8–10.9, average 7.1). Both have $[Tb/Yb]_N$ ratios >1, averaging 2.23 for GF-peridotite and 1.79 for Grt-peridotite, which suggests that garnet was not a residual phase. Compositional and mineralogical data suggest that the Zhimafang peridotite represents a fragment of harzburgite-type depleted mantle, i.e. orthopyroxene and olivine were the only original silicate minerals in the rock. Random and high contents of K_2O and enriched-LREE are not features typical of depleted mantle, but may be a result of metasomatism (Zhang *et al*., 2007).

Titania contents are low in both types of peridotite, mostly <0.05 wt%. Abundances of <0.2 wt% are typical of low-temperature (<1100 °C) garnet peridotite (Boyd, 1989).

MINERAL COMPOSITIONS

The mineralogies and textures of the Zhimafang peridotites described above indicate a complicated petrological history involving at least three stages of mineral growth: (i) most equigranular minerals, such as olivine, Opx, Cpx and garnet and/or porphyroblastic garnet; (ii) amphibolite facies retrograde metamorphism, and (iii) greenschist facies overprint. In addition, the presence of early minerals, such as olivine and chromite, as inclusions in other minerals suggest an earlier stage of mineral growth and some granular phlogopite suggests an early metasomatic stage.

Mineral compositions were mostly analysed with a JEOL superprobe 733 equipped with five wavelength-dispersive spectrometers at Stanford University. Operating conditions were 15 kV and 12 nA or 18 nA beam current. The electron beam was $\sim$0.5 μm, and the counting time was 20 s. Some additional analyses were carried out at the Institute of Geology and Geophysics, Chinese Academy of Science, Beijing. Total iron is expressed as FeO. The Fe^{3+} content of amphibole was estimated by the method of Schumacher (1991), and that in chromite was calculated from charge balance, assuming total cations to be 3. The compositions of representative minerals from the Zhimafang peridotite are listed in Table 3.

Olivine

Olivine ranges in composition from Fo_{89} to Fo_{93} (mostly 91–93); that from the GF-peridotite has a higher Fo content (92–93 mol.%) but lower SiO_2 (<41 wt%) than that from the Grt-peridotite (Fo_{91-93}).

© 2007 Blackwell Publishing Ltd

Table 3. Representative compositions of minerals in the Zhimafang peridotite

	Grt-perid.	Grt-perid.	Grt-perid.	Grt-perid.	Grt-perid.	Grt-perid.	Grt-perid.	Grt-perid.	Grt-perid.	Grt-perid.	Grt-perid.	Grt-perid.	Grt-perid.	Grt-perid.	Grt-perid.	Grt-perid.	Grt-perid.	Grt-peridotite
Sample:	C21-132-53	C21-132-53	C21-132-53	C21-134-55	C21-134-55	C21-134-55	C21-134-55	C21-134-55	C21-134-55	C25-143-61	C25-143-61	C25-143-61	C25-143-61	C25-143-61	C27-144-63	C27-144-63	C27-144-63	C27-144-63lher*	c34-150-73
Mineral:	opx	grt	grt sm	opx	opx	opx	grt sm	grt sm	grt sm	opx	grt sm	grt sm	grt lg	grt-lg	opx	opx	grt sm	grt sm	Ol
Point:	/2-1	/5-4	/3-1	/4-1	/7-1	/1-1	/3-1	/2-1	/10-1 core	/2-1	403 core	404 rim	394 rim	395 rim	/5-1	/4-2	/5-2	196	2-4
SiO_2	58.87	40.10	42.23	57.14	57.72	58.67	40.72	41.26	42.03	57.35	41.22	41.48	42.01	42.00	56.68	57.63	40.43	42.31	41.71
TiO_2	0.01	0.02	0.16	0.09	0.00	0.03	0.10	0.10	0.10	0.02	0.00	0.03	0.00	0.05	0.00	0.00	0.00	0.00	0.00
Al_2O_3	0.18	22.63	22.56	0.18	0.17	0.17	22.79	22.17	22.36	0.09	21.37	21.74	22.83	22.74	0.18	0.18	21.96	22.00	0.00
Cr_2O_3	0.00	2.35	2.27	0.12	0.13	0.06	1.81	2.40	2.33	0.04	2.77	2.44	1.28	1.35	0.07	0.06	2.54	2.28	0.00
Fe_2O_3	0.00	0.00	0.00	2.74	2.45	0.00	0.00	0.00	0.00	1.16					0.00	0.00	0.00		
FeO	5.29	8.23	8.72	2.66	3.08	5.03	10.97	11.00	8.56	5.09	11.33	10.78	10.16	9.85	4.58	4.62	11.00	10.23	8.12
MnO	0.16	0.40	0.35	0.17	0.05	0.14	0.73	0.73	0.42	0.10	0.53	0.52	0.41	0.38	0.14	0.09	0.69	0.61	0.00
MgO	35.55	20.39	19.18	36.74	36.91	36.00	19.04	17.91	19.42	35.43	18.40	18.47	19.16	19.36	37.14	36.84	18.39	18.31	50.38
NiO		0.00	0.00				0.00	0.02	0.07								0.00		
CaO	0.10	5.02	5.23	0.06	0.02	0.07	4.40	5.04	5.36	0.11	4.19	4.22	4.65	4.77	0.11	0.00	4.83	4.65	0.00
K_2O	0.00	0.03	0.04	0.01	0.00	0.00	0.04	0.01	0.02	0.00	0.01	0.03	0.04	0.03	0.00	0.03	0.01	0.00	0.00
NaO	0.02	0.00	0.04	0.00	0.01	0.02	0.00	0.00	0.00	0.00	0.01	0.00	0.00	0.00	0.01	0.05	0.00	0.00	0.00
Total	100.23	99.18	100.78	99.90	100.57	100.17	100.60	100.64	100.67	99.51	99.83	99.71	100.54	100.53	99.01	99.64	99.87	100.38	100.20
Si	2.01	2.87	3.00	1.96	1.96	2.00	2.91	2.97	2.99	1.98	2.99	3.00	2.99	2.99	1.95	1.97	2.92	3.03	1.01
Ti	0.00	0.00	0.01	0.00	0.00	0.00	0.01	0.01	0.01	0.00	0.00	0.00	0.00	0.00	0.00	0.00	0.00	0.00	0.00
Al	0.00	0.13	0.13	0.00	0.00	0.00	0.10	0.14	0.13	0.00	0.16	0.14	0.07	0.08	0.00	0.00	0.15	0.13	0.00
Cr	0.01	1.91	1.89	0.01	0.01	0.01	1.92	1.88	1.87	0.00	1.83	1.85	1.92	1.91	0.01	0.01	1.87	1.86	0.00
Fe	0.15	0.21	0.00	0.15	0.15	0.14	0.16	0.05	0.02	0.18					0.13	0.13	0.14	0.00	0.16
Mn	0.01	0.02	0.02	0.01	0.00	0.00	0.04	0.04	0.03	0.00	0.03	0.03	0.02	0.02	0.00	0.00	0.04	0.04	0.00
Mg	1.81	2.18	2.03	1.88	1.87	1.83	2.03	1.92	2.06	1.83	1.99	1.99	2.04	2.06	1.90	1.88	1.98	1.96	1.82
Ni	0.00	0.39	0.40	0.00	0.00	0.00	0.34	0.39	0.41	0.00	0.33	0.33	0.36	0.36	0.00	0.00	0.37	0.36	
Ca		0.00	0.00				0.00	0.00	0.00								0.00		0.00
K	0.00	0.00	0.00	0.00	0.00	0.00	0.00	0.00	0.00	0.00	0.00	0.00	0.00	0.00	0.00	0.00	0.00	0.00	0.00
Na	0.00	0.00	0.01	0.00	0.00	0.00	0.01	0.00	0.00	0.00	0.00	0.00	0.01	0.00	0.00	0.00	0.00	0.00	0.00
Fo																			91.71
Fa																			8.29
En	0.92			0.93	0.93	0.93				0.91					0.93	0.93			
Fs	0.08			0.07	0.07	0.07				0.09					0.06	0.07			
Wo	0.00			0.00	0.00	0.00				0.00					0.00	0.00			
uv:		9.30	8.60				7.00	9.20	8.80		7.85	6.97	3.58	3.76			9.90	8.70	
ad:		14.80	0.00				11.00	3.10	1.10		0.00	0.00	0.00	0.00			9.80	0.00	
gr:		0.00	4.80				0.00	0.80	3.80		2.88	3.92	8.17	8.25			0.00	3.30	
py:		75.90	68.40				69.80	64.70	69.00		65.55	66.33	67.38	67.86			67.90	66.00	
sp:		0.80	0.70				1.50	1.50	0.80		1.07	1.06	0.82	0.76			1.40	1.20	
al:		9.80	17.50				17.10	20.70	16.50		22.65	21.72	20.05	19.37			17.90	20.70	

	Grt-peridotite	Grt-perid.	Grt-perid.	Grt-perid.	Grt-perid.	Grt-peridotite	Grt-peridotite	Grt-peridotite	Grt-peridotite	Grt-peridotite	Grt-perid.	Grt-perid.	Grt-perid.	Grt-perid.	Grt-perid.	Grt-perid.	Grt-perid.	Grt-perid.	Grt-perid.
Sample:	c34-150-73	c34-150-73	c34-150-73	C34-150-73	C34-150-73	c34-151-74	c34-151-74	c34-151-74	c34-151-74	c34-151-74	c34-151-74	c34-151-74	C34-151-74	C34-151-74	C34-151-74	C38-157-80	C38-157-80	C40-158-82	C40-158-82
Mineral:	Ol	opx	opx	grt-sm	grt-sm	Ol	Ol	Ol	Ol	Ol	opx	opx	grt-sm	grt-sm	grt-sm	cpx	opx	cpx	opx
Point:	19	1-3.	14-2.	3-3-rim	.3-2	2-4.	2-5.	6-10.	7-3.	8-5.	10-1.	4-1.	9-1.	96 rim	97 core	/2-1-cpx	/3-1-opx	/3-1-cpx	/2-1-opx
SiO_2	41.14	58.54	59.35	40.41	40.83	41.62	41.56	41.08	41.43	41.37	59.07	58.10	41.05	42.48	42.21	54.21	57.44	54.14	58.35
TiO_2	0.00	0.00	0.00	0.02	0.01	0.00	0.00	0.16	0.00	0.00	0.00	0.00	0.00	0.02	0.02	0.07	0.00	0.02	0.00
Al_2O_3	0.00	0.00	0.00	22.14	21.62	0.00	0.00	0.00	0.00	0.00	0.00	0.00	21.31	22.73	22.49	0.25	0.21	0.26	0.16
Cr_2O_3	0.00	0.00	0.00	2.27	2.76	0.00	0.00	0.00	0.00	0.00	0.00	0.18	2.37	1.89	2.03	0.34	0.00	0.38	0.09
Fe_2O_3				0.00	0.00											2.35	2.43	1.80	1.58
FeO	8.76	5.41	4.97	11.59	11.67	8.86	8.62	8.59	8.52	8.66	5.50	5.73	11.64	10.42	9.61	0.00	2.67	0.00	3.40

© 2007 Blackwell Publishing Ltd

© 2007 Blackwell Publishing Ltd

Table 3. *Cont'd*

	Grt-peridotite	Grt-perid.	Grt-perid.	Grt-perid.	Grt-perid.	Grt-peridotite	Grt-peridotite	Grt-peridotite	Grt-peridotite	Grt-peridotite	Grt-perid.	Grt-perid.	Grt-perid.	Grt-perid.	Grt-perid.	Grt-perid.	Grt-perid.	Grt-perid.	Grt-perid.
Sample:	c34-150-73	c34-150-73	c34-150-73	C34-150-73	C34-150-73	c34-151-74	c34-151-74	c34-151-74	c34-151-74	c34-151-74	c34-151-74	c34-151-74	C34-151-74	C34-151-74	C34-151-74	C38-157-80	C38-157-80	C40-158-82	C40-158-82
Mineral:	Ol	opx	opx	grt-sm	grt-sm	Ol	Ol	Ol	Ol	Ol	opx	opx	grt-sm	grt-sm	grt-sm	cpx	opx	cpx	opx
Point:	19	1-3.	14-2.	3-3-rim	.3-2	2-4.	2-5.	6-10.	7-3.	8-5.	10-1.	4-1.	9-1.	96 rim	97 core	/2-1-cpx	/3-1-opx	/3-1-cpx	/2-1-opx
MnO	0.00	0.00	0.00	0.78	0.86	0.00	0.00	0.00	0.00	0.00	0.00	0.00	0.00	0.53	0.52	0.06	0.13	0.11	0.20
MgO	49.70	36.83	36.33	17.71	17.16	49.80	50.17	50.11	50.31	50.38	36.14	35.71	17.98	17.97	18.56	17.80	36.95	17.34	36.99
NiO				0.05	0.03														
CaO	0.00	0.12	0.00	4.74	5.47	0.00	0.00	0.00	0.00	0.00	0.11	0.00	4.72	4.62	4.63	24.60	0.00	24.59	0.10
K_2O	0.00	0.00	0.00	0.00	0.00	0.00	0.00	0.00	0.00	0.00	0.00	0.00	0.00	0.00	0.03	0.01	0.00	0.03	0.00
NaO	0.00	0.00	0.00	0.00	0.00	0.00	0.00	0.00	0.00	0.00	0.00	0.00	0.00	0.00	0.01	0.50	0.00	0.51	0.02
Total	99.60	100.90	100.65	99.71	100.41	100.28	100.35	99.94	100.26	100.41	100.83	99.72	99.07	100.66	100.11	100.24	99.86	99.18	100.94
Si	1.00	1.99	2.01	2.93	2.96	1.01	1.01	1.00	1.00	1.00	2.00	2.00	6.00	3.03	3.02	1.96	1.96	1.98	1.98
Ti	0.00	0.00	0.00	0.00	0.00	0.00	0.00	0.00	0.00	0.00	0.00	0.00	0.00	0.00	0.00	0.00	0.00	0.00	0.00
Al	0.00	0.00	0.00	0.13	0.16	0.00	0.00	0.00	0.00	0.00	0.00	0.00	0.27	0.11	0.12	0.01	0.00	0.01	0.00
Cr	0.00	0.00	0.00	1.89	1.85	0.00	0.00	0.00	0.00	0.00	0.00	0.01	3.67	1.91	1.90	0.01	0.01	0.01	0.01
Fe	0.18	0.15	0.14	0.11	0.08	0.18	0.17	0.17	0.17	0.18	0.16	0.16	1.42	0.00	0.00	0.06	0.14	0.05	0.14
Mn	0.00	0.00	0.00	0.05	0.05	0.00	0.00	0.00	0.00	0.00	0.00	0.00	0.00	0.03	0.03	0.00	0.00	0.00	0.01
Mg	1.81	1.87	1.84	1.92	1.85	1.80	1.81	1.82	1.82	1.82	1.83	1.83	3.92	1.91	1.98	0.96	1.88	0.95	1.87
Ni		0.00	0.00	0.37	0.42						0.00	0.00	0.74	0.35	0.36	0.95	0.00	0.96	0.00
Ca	0.00			0.00	0.00	0.00	0.00	0.00	0.00	0.00									
K	0.00	0.00	0.00	0.00	0.00	0.00	0.00	0.00	0.00	0.00	0.00	0.00	0.00	0.00	0.00	0.00	0.00	0.00	0.00
Na	0.00	0.00	0.00	0.00	0.00	0.00	0.00	0.00	0.00	0.00	0.00	0.00	0.00	0.00	0.00	0.04	0.00	0.04	0.00
Fo	91.00					90.93	91.22	91.23	91.33	91.21									
Fa	9.00					9.07	8.78	8.77	8.67	8.79									
En		0.92	0.93								0.92	0.92				0.49	0.93	0.48	0.93
Fs		0.08	0.07								0.08	0.08				0.03	0.07	0.03	0.07
Wo		0.00	0.00								0.00	0.00				0.48	0.00	0.49	0.00
uv:				8.90	10.70								6.83	7.30	7.80				
ad:				7.10	5.40								1.40	0.00	0.00				
gr:				0.00	0.00								4.04	4.80	4.30				
py:				65.40	62.70								65.02	65.50	67.30				
sp:				1.60	1.80									1.10	1.10				
al:				20.40	21.20								22.67	21.30	19.60				

	Grt-perid.	Grt-perid.	Grt-perid.	Grt-perid.	Grt-perid.	Grt-peridotite	Grt-peridotite	Grt-perid.	Grt-perid.	GF-perid.	GF-perid.	Grt-perid.	Grt-perid.	GF-perid.	GF-perid.	GF-perid.
Sample:	c30-164-87	c30-164-87	c30-164-87	c30-164-87	c30-164-87	c46-164-87	c46-164-87	C46-164-87	C46-164-87	C47-165-90	C47-165-90	C47-165-90	C47-165-90	C51-167-94	C51-167-94	C51-167-95
Mineral:	cpx	cpx	cpx	opx	opx	Ol	Ol	grt-sm	grt-sm	cpx	opx	Grt-lg	Grt-lg	cpx	opx	opx
Point:	7-1(core)	7-2(rim)	2-1(inol)	6-1(core)	6-2(rim)	2-3(core)	2-4(rim)	1-1 c	1-2 r			rim	core			
SiO_2	53.95	51.66	53.28	57.68	58.38	41.36	41.01	41.76	41.67	54.64	58.47	42.04	42.12	55.57	58.71	58.85
TiO_2	0.07	0.06	0.06	0.04	0.00	0.08	0.04	0.02	0.01	0.00	0.00	0.00	0.00	0.05	0.05	0.05
Al_2O_3	2.29	2.18	1.73	0.10	0.19	0.00	0.00	21.41	21.33	1.49	0.08	22.87	22.79	0.50	0.06	0.20
Cr_2O_3	1.80	1.88	2.21	0.07	0.13	0.18	0.32	1.98	2.23	2.04	0.07	1.42	1.63	0.83	0.00	0.08
Fe_2O_3								1.31	1.12							
FeO	2.60	5.35	3.04	4.12	4.14	6.67	6.74	8.26	8.60	2.27	4.67	10.10	9.14	1.74	4.37	5.21
MnO	0.00	0.00	0.32	0.04	0.01	0.00	0.00	0.41	0.54	0.05	0.08	0.71	0.35	0.09	0.18	0.13
MgO	15.21	15.44	15.06	36.92	36.64	50.91	51.45	19.60	19.35	15.62	37.13	19.73	20.00	17.14	37.09	35.62
NiO						0.66	0.59	0.00	0.03							
CaO	20.78	20.80	20.36	0.07	0.06	0.02	0.00	4.77	4.64	21.08	0.08	4.03	4.55	24.03	0.07	0.10
K_2O	0.03	0.04	0.00	0.04	0.02	0.00	0.00	0.04	0.04	0.00	0.00	0.05	0.02	0.00	0.01	0.00
NaO	2.42	2.33	2.48	0.04	0.04	0.01	0.00	0.01	0.02	2.38	0.01	0.00	0.00	0.85	0.02	0.00
Total	99.72	100.49	99.01	99.44	99.85	99.89	100.15	99.58	99.57	99.57	100.59	100.95	100.60	100.80	100.56	100.24

Table 3. *Cont'd*

	Grt-perid.	Grt-perid.	Grt-perid.	Grt-perid.	Grt-perid.	Grt-peridotite	Grt-peridotite	Grt-perid.	Grt-perid.	GF-perid.	GF-perid.	Grt-perid.	Grt-perid.	GF-perid.	GF-perid.	GF-perid.
Sample:	c30-164-87	c30-164-87	c30-164-87	c30-164-87	c30-164-87	c46-164-87	c46-164-87	C46-164-87	C46-164-87	C47-165-90	C47-165-90	C47-165-90	C47-165-90	C51-167-94	C51-167-94	C51-167-95
Mineral:	cpx	cpx	cpx	opx	opx	Ol	Ol	grt-sm	grt-sm	cpx	opx	Grt-lg	Grt-lg	cpx	opx	opx
Point:	7-1(core)	7-2(rim)	2-1(inol)	6-1(core)	6-2(rim)	2-3(core)	2-4(rim)	1-1 c	1-2 r			rim	core			
Si	1.96	1.89	1.96	1.98	1.99	1.00	0.99	6.01	6.01	1.99	1.99	2.98	2.98	2.00	1.99	2.01
Ti	0.00	0.00	0.00	0.00	0.00	0.00	0.00	0.00	0.00	0.00	0.00			0.00	0.00	0.00
Al	0.10	0.09	0.08	0.00	0.01	0.00	0.00	0.23	0.25	0.06	0.00	0.08	0.09	0.02	0.00	0.00
Cr	0.05	0.05	0.06	0.00	0.00	0.00	0.01	3.63	3.62	0.06	0.00	1.91	1.90	0.02	0.00	0.01
Fe	0.08	0.16	0.09	0.12	0.12	0.14	0.14	0.14	0.12	0.07	0.13	0.07	0.04	0.05	0.12	0.15
Mn	0.00	0.00	0.01	0.00	0.00	0.00	0.00	0.05	0.07	0.00	0.00	0.04	0.02	0.00	0.01	0.00
Mg	0.82	0.84	0.83	1.89	1.86	1.84	1.86	4.20	4.16	0.85	1.88	2.08	2.11	0.92	1.88	1.81
Ni	0.81	0.82	0.80	0.00	0.00			0.74	0.72	0.82	0.00	0.31	0.35	0.93	0.00	0.00
Ca						0.00	0.00	0.00	0.00							
K	0.00	0.00	0.00	0.00	0.00	0.00	0.00	0.00	0.00	0.00	0.00			0.00	0.00	0.00
Na	0.17	0.17	0.18	0.00	0.00	0.00	0.00	0.01	0.01	0.17	0.00	0.01	0.00	0.06	0.00	0.00
Fo						93.18	93.16									
Fa						6.85	6.84									
En	0.48	0.46	0.48	0.94	0.94					0.49	0.93			0.48	0.94	0.92
Fs	0.05	0.09	0.05	0.06	0.06					0.04	0.07			0.03	0.06	0.08
Wo	0.47	0.45	0.47	0.00	0.00					0.47	0.00			0.49	0.00	0.00
uv:								5.65	6.38			0.00	0.00			
ad:								3.61	3.07			4.40	2.80			
gr:								3.02	2.53			0.50	2.70			
py:								70.28	69.56			70.30	70.90			
sp:								0.83	1.11			1.40	0.70			
al:								16.62	17.36			18.00	16.80			

sm, small garnet; lg, large garnet.

© 2007 Blackwell Publishing Ltd

Pyroxene

Both the Grt-peridotite and GF-peridotite have higher abundance of enstatite (average 10 vol.%) than diopside (1–5 vol.%). Diopside has high $Mg^{\#}$ members (0.93–0.95), a considerable amount of Cr_2O_3 (0.38–2.09 wt%, mostly 1–2 wt%), and variable Al_2O_3 (0.2–2.3 wt%) and Na_2O (0.5–2.5 wt%). Because Na_2O in Cpx is a pressure-dependent element, it has been plotted against other important elements (Fig. 6). These diagrams show that Na_2O is correlated positively with both Al_2O3 and Cr_2O_3, but negatively with CaO and MgO. It shows no linear relationship with SiO_2. Two groups of Cpx are distinguished: (i) $Na_2O > 1.5$ wt%, and (ii) $Na_2O < 1$ wt%. The high-Na_2O Cpx also has high contents of Al_2O_3 (1–2.3 wt%) and Cr_2O_3 (mostly > 1.2), but low MgO (11–16.5) and CaO (20–22.5). This Cpx forms large grains in the peridotite and small inclusions in olivine. The low-Na_2O Cpx is characterized by low Al_2O_3 (0.2–0.8), low Cr_2O_3 (0.3–0.7), high MgO (17–17.8) and high CaO (23.7–24.6) (Fig. 6).

The Opx is enstatite (En_{92-93}) with quite variable MgO (33.3–37.5 wt%) and SiO_2 (56.7–60.2 wt%), and contains only trace amounts of Cr_2O_3 (0–0.1 wt% except for one up to 0.3 wt%) and Al_2O_3 (0–0.3 wt%). Enstatite in both the Grt-peridotite and GF-peridotite shows similar compositional ranges, although the analyses are limited.

Garnet

Garnet from both lherzolites and harzburgites is Cr-bearing pyrope ($Ura_{4-12}Prp_{62-73}Alm_{14-24}Grs_{1-10}Sps_{0-2}$). The Cr_2O_3 content (1.28–4.23 wt%) of the garnet varies from sample to sample. Consistent with the petrography, there are two compositional groups of garnet. The early-formed varieties, including mainly equigranular garnet and the cores of some large grains, have high Cr_2O_3 contents (up to ~4 wt%), whereas the porphyroblastic garnet mainly has low Cr_2O_3 (maximum of 2 wt%). However, Al_2O_3 (21–24 wt%), SiO_2 (42–43 wt%) and MgO (19–21 wt%) contents are all higher in late garnet than in the early ones (Fig. 7). Zoning is best developed in the equigranular garnet, e.g. Cr_2O_3, MgO and Al_2O_3 contents in an equigranular garnet, vary from centre to rim, from 3.4 to 4.2 wt%, 18.4 to 17.5 wt% and from 21.1 to 20.1 wt%, respectively. Titania is very low in all garnet, mostly < 0.05 wt%. A TiO_2 content < 0.2 wt% is considered to be one of the features of low-temperature (< 1100 °C) garnet peridotite (Boyd, 1989).

Chromite or chromium-spinel

Chromite or chromium (Cr)-spinel is an important accessory mineral in both the Grt- and GF-peridotite, where it commonly occurs as inclusions in olivine, Opx, Cpx and garnet. The chromite is characterized by high contents of Cr_2O_3 and FeO, 49–58 wt% and 33–43 wt%, respectively, in Grt-peridotite, and 49–52 wt% and 24–26 wt%, respectively, in GF-peridotite. Al_2O_3 contents are very low in grains of both rock types, 3–9 wt% in Grt-peridotite and 2–4 wt% in GF-peridotite. Chromites have high Cr/(Al + Cr) ratios (0.76 to 0.99) and low $Mg^{\#}$ (0.21–0.35), and consist mainly of four components: $FeCr_2O_4$, $MgCr_2O_4$, Fe_3O_4 or $MgAl_2O_4$. There are some transitional compositions between $(FeMg)Cr_2O_4$ and Fe_3O_4, in which the magnetite component ranges from 40% to 62%. These are all secondary phases, which occur with phlogopite and chlorite replacing garnet. In the $100Mg/(Mg + Fe^{2+})$ *v.* $100Cr/(Cr + Al)$ diagram, both types plot away from the region of ophiolitic ultramafic rocks, but close to the region of iron-rich Alpine-type peridotite (Fig. 8). No zoning in chromite was observed in grains either from Grt- or GF-peridotite.

Hydrous phases and carbonate

Phlogopite is the dominant hydrous mineral in the Zhimafang peridotites, and is characterized by high MgO (24.95–26.15 wt%; $Mg^{\#}$ 0.95) and low FeO (2.02–2.66 wt%) and TiO_2 (0.04–0.12 wt%). The phlogopite in the garnet-phlogopite-amphibole vein is similar to that in the peridotite, but it has slightly higher FeO (3.04 wt%) and lower $Mg^{\#}$ (0.94).

Ti-clinohumite is a dense hydrous magnesium silicate in the mantle that may be stable at 150–300 km (5–10 GPa) and 700–1100 °C (Ahrens, 1989). The TiO_2 contents of Ti-clinohumite in the peridotite (1.96–3.58 wt%) vary with its occurrence. The highest TiO_2 contents are in exsolution lamellae of Ti-chondrodite (4.82–7.19 wt%) and Ti-clinohumite (7.57–8.62 wt%) that occur in a diopside inclusion within coarse-grained garnet (Xu *et al.*, 2003). Ratios of (Mg + Fe + Ti)/Si are ~2.22, slightly lower than that of ideal statistical clinohumite. No F was detected in this mineral.

Magnesite

Magnesite occurs in a number of peridotite samples as large megacrysts and smaller groundmass grains. Many of the megacrysts contain inclusions of phlogopite (common) and Ti-clinohumite (rare). Magnesite is nearly Ca-free (CaO = 0.06–0.23 wt%) and has high $Mg^{\#}$ (0.93–0.95). It is rimmed by aggregates of dolomite ± calcite that probably formed during decompression. The retrograde dolomite contains 0.76–0.89 wt% FeO, and calcite contains minor MnO (1.25 wt%) and MgO (1.61 wt%).

Retrograde amphibole

The retrograde amphibole replacing garnet has compositions different from that replacing diopside. The symplectite after garnet contains pargasite with high

© 2007 Blackwell Publishing Ltd

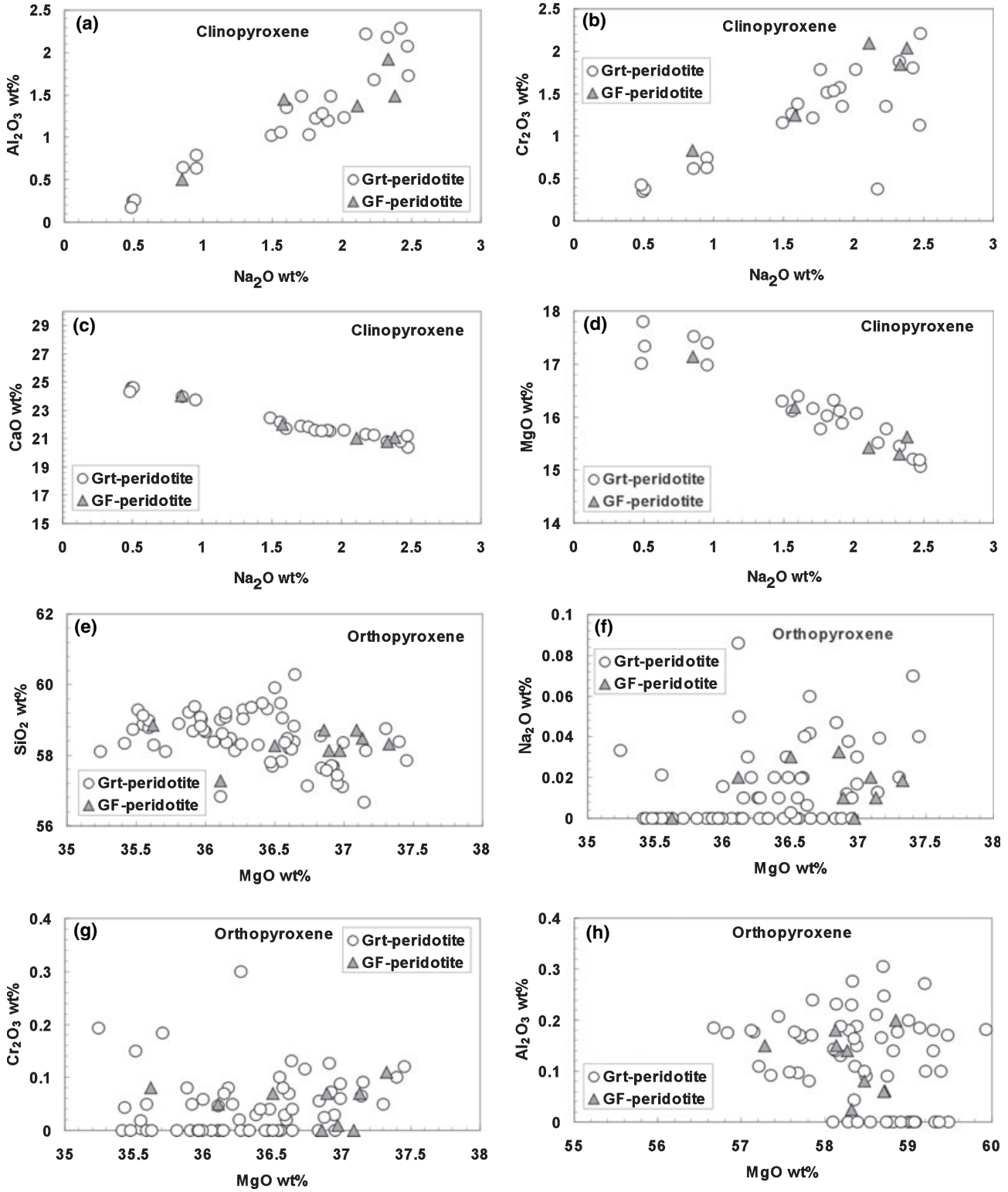


Fig. 6. Compositional variations for diopside and enstatite in Grt- and GF-peridotite which show similar and wide ranges in composition; Na_2O shows a positive relation with Al_2O_3 and Cr_2O_3 and a negative relation with MgO and CaO.

© 2007 Blackwell Publishing Ltd

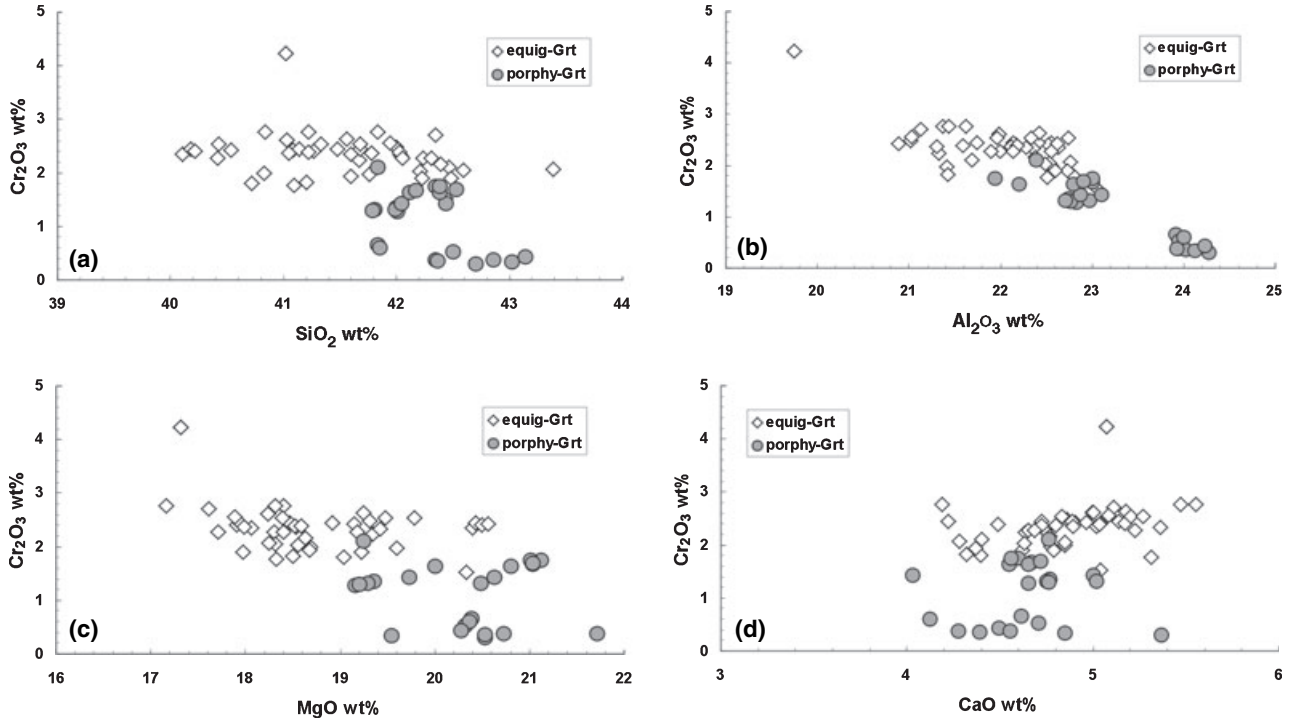


Fig. 7. Compositional variation in porphyroblastic garnet (Lg-grt) and equigranular garnet (Sm-grt) in Grt-peridotite. The Sm-grt have relatively higher contents of Cr_2O_3 and lower contents of Al_2O_3, MgO and SiO_2 than the Lg-grt.

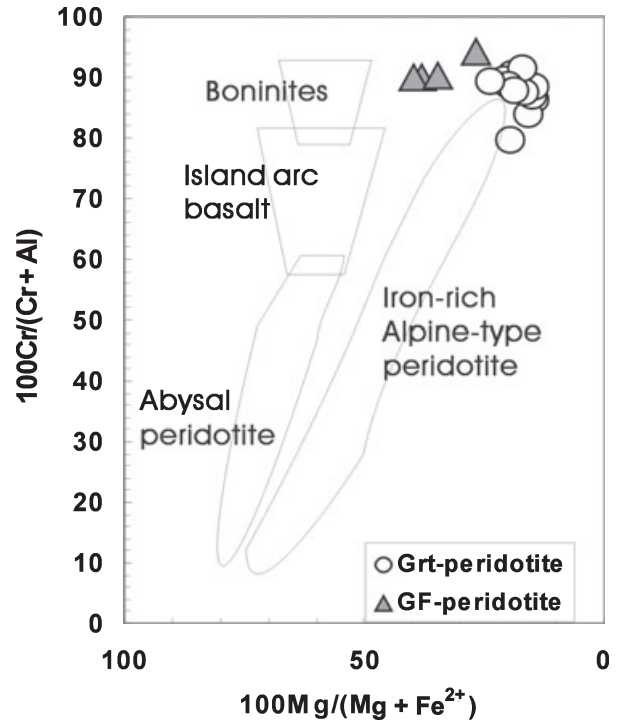


Fig. 8. 100Cr/(Cr + Al) *v.* 100Mg/(Mg + Fe) plot for chromite in both the Grt- and GF-peridotite, which has high 100Cr/(Cr + Al); that in the Grt-peridotite has somewhat higher 100Mg/(Mg + Fe^{2+}) than the GF-peridotite, and both are plot away from tectonically known regions.

$Mg^{\#}$ (0.91–0.95). Some of these grains have Ca < 1.5, and all the Na and K occurs in the A site. The amphibole replacing diopside is tremolite, which contains very minor FeO (< 0.3 wt%) and Na_2O. Chlorite after garnet contains minor Cr_2O_3, up to 2.0 wt%.

PEAK METAMORPHIC CONDITIONS

General considerations

For peridotites, a relatively large number of thermobarometers is available (for a discussion see Krogh Ravna & Paquin, 2003). Unfortunately, most of them are based on experiments that were not reversed. However, Brey & Köhler (1990) presented a set of reversed experiments in different bulk systems that provide a basis for both the assessment of pre-existing thermobarometers and the formulation of new, internally consistent thermobarometers for peridotites (Brey & Köhler, 1990). In addition, Brey *et al.* (1999) presented experimental results for garnet-spinel-olivine-orthopyroxene equilibria in the system FeO-MgO-Al_2O_3-SiO_2-Cr_2O_3 (FMASCr) and showed that the distribution of Cr and Al between spinel and garnet in equilibrium with Opx and Ol may be used as a thermobarometer (Girnis & Brey, 1999).

In this study, the following geothermobarometers are used: (i) $T_{2pxBK90}$, the two-pyroxene thermometer based on the exchange of enstatite and diopside components between coexisting orthopyroxene and clin-

© 2007 Blackwell Publishing Ltd

opyroxene as calibrated by Brey & Köhler (1990); (ii) $T_{Ca\text{-}opx}$, the Ca-in-orthopyroxene thermometer (Brey & Köhler, 1990); (iii) $T_{Grt\text{-}CpxK88}$, the thermometer based on the partitioning of Fe and Mg between garnet and clinopyroxene (Krogh, 1988; see discussion in Brey & Köhler, 1990); (iv) $T_{Grt\text{-}OpxBK90}$, the thermometer based on the partitioning of Fe and Mg between garnet and orthopyroxene (Brey & Köhler, 1990); (v) $T_{Grt\text{-}OlONW79}$, the thermometer based on the partitioning of Fe and Mg between garnet and Opx (O'Neill & Wood, 1979, corrected by O'Neill & Wood, 1980); (vi) $P_{Al\text{-}in\text{-}opxBK90}$, the barometer based on the Al content of Opx coexisting with garnet (Brey & Köhler, 1990). In addition, the partitioning of Cr and Al between spinel and garnet in equilibrium with olivine and Opx was used to constrain peak pressure and temperature.

Fe-Mg exchange thermometry is generally fraught with uncertainties in the $Fe^{3+}/\Sigma Fe$ ratios of both natural phases and the phases from which the thermobarometers were calibrated in the original experiments. For peridotites, it has been assumed that the experiments used to calibrate these thermometers produced garnet, orthopyroxene and clinopyroxene with substantial Fe^{3+} content, similar to those of natural samples. In natural garnet-bearing peridotites, $Fe^{3+}/\Sigma Fe$ ratios increase in the order olivine (~0.00), garnet (~0.02–0.05), orthopyroxene (~0.03–0.10) and clinopyroxene (0.15–0.40), and the $Fe^{3+}/\Sigma Fe$ in garnet increases significantly with increasing P–T (e.g. Brey & Köhler, 1990; Luth *et al.*, 1990; Luth & Canil, 1993; Canil & O'Neill, 1996; Smith, 1999). Because of the large uncertainty of the $Fe^{3+}/\Sigma Fe$ ratios in pyroxene, exchange thermometers may yield false temperature values that are likely to be too high. On the other hand, olivine and garnet are the minerals with the lowest $Fe^{3+}/\Sigma Fe$ ratios. Therefore, the exchange thermometer $T_{Grt\text{-}OlONW79}$ should yield more reliable temperatures.

Pyroxene solvus relationships at low temperatures (< 900 °C) are not well constrained, because of the steepening of the solvus limbs at successively lower temperatures. In this case, calculated temperatures ($T_{2pxBK90}$, $T_{Ca\text{-}opx}$) may not be reliable, in particular in the case of Na-rich pyroxene compositions. Furthermore, if Cpx is present in only small amounts, the Ca content in Opx may be lower than the maximum content indicated by the solvus, because of chemical subsystems with and without Cpx as a source for Ca. Furthermore, if the Al content in orthopyroxene is small, pressure values calculated with $P_{Al\text{-}in\text{-}opxBK90}$ may not be reliable because of analytical uncertainties. For the garnet peridotites investigated in this study, an upper pressure limit of ~6.0 GPa is given by the fact that: (i) garnet does not contain a detectable amount of a majorite component and (ii) there is no textural evidence for exsolution of pyroxene from garnet (see Irifune, 1987).

One relevant assumption for calculation of peak metamorphic pressures and temperatures in UHP peridotites is that core compositions of coexisting mineral grains reflect the peak metamorphic conditions and therefore indicate frozen-in equilibrium. However, during retrograde evolution, elements with high diffusivity, such as Fe and Mg, will most probably undergo diffusive relaxation and this will result in retrograde zonation patterns. If such retrograde compositions are used for thermometric calculations, unrealistically low peak temperatures are obtained. On the other hand, it is certainly possible that during rapid prograde metamorphism, low-diffusivity elements may not have equilibrated at peak metamorphic conditions, resulting in calculated temperature values that are too low.

Results of thermobarometric calculations

Temperature and pressure values obtained for the investigated peridotites are given in Table 4. Calculated temperatures based on two-pyroxene solvus relationships are generally (very) low ($T_{2pxBK90} \leq 718$ °C and ≤732 °C; $T_{Ca\text{-}opx} = 582$–791 and 611–827 °C, at 5.0 and 6.0 GPa, respectively). Although these low temperature values may not be reliable, the very low Ca contents in orthopyroxene and the relatively high values of Ca/(1 − Na) (in cations per formula unit) of

Table 4. Metamorphic P–T conditions of PP1 peridotite

	T Grt-Opx[a]		*T* Ca-in-Opx[a]		*T* 2Px[a]		*T* Grt-Cpx[c]		*T* Grt-Ol[b]		*P* Al-in-Opx[a]	
	5.0 GPa	6.0 GPa	5.0 GPa	6.0 GPa	5.0 GPa	6.0 GPa	5.0 GPa	6.0 GPa	5.0 GPa	6.0 GPa	800°C	1000°C
C21-132-53	896–999	955–1063	766	801							5.02–5.13	6.77–6.98
C21-134-55	686–952	735–1014	582–701	611–734							5.73–5.82	7.71–8.01
C25-143–61	798–929	852–989	782	818							*7.14–7.46*	*9.95-10.05*
C25-144-63	*642–711*	*689–761*	782	818							4.98–5.29	6.96–7.19
C30-164-87			700–720	733–753	*352–607*	*363–619*						
C34-150-73	*632–680*	*678–729*	791	827					*594–643*	*614–658*	5.47–5.67	7.64–8.06
C34-151-74	703–920	752–981	778	814					615–773	634–775	5.40–5.58	7.54–7.62
C38-157-80					*287*	*294*						
C40-158-82			765	801								
C46-164-87									*663–691*	*676–701*		
C47-165-90	721–1016	771–1081	719–736	752–771	*429–718*	*438–732*	807–1094	843–1139			5.10–5.55	6.83–7.44
C51-167-94			677–766	710–801	*521–525*	*531–535*						

Temperatures calculated at 5 and 6 GPa.
[a]Brey & Köhler (1990); [b]O'Neill & Wood (1979); [c]Krogh (1988).

© 2007 Blackwell Publishing Ltd

clinopyroxene suggest that peak temperatures were below 900 °C, provided that equilibration was achieved during prograde metamorphism. Temperature values obtained from the $T_{\text{Grt-OlONW79}}$ thermometer (< 820 °C; Table 4) are in line with this assumption. On the other hand, temperature values calculated from Fe-Mg partitioning between garnet and orthopyroxene ($T_{\text{Grt-OpxBK90}}$) show a large spread and range from 632 to 1151 °C (at 5.0 GPa). Likewise, values obtained from $T_{\text{Grt-CpxK88}}$ range from 807 to 1094 °C (at 5.0 GPa). The scatter in values obtained by both thermometers is, in part, due to retrograde garnet compositions (i.e. relatively low X_{Mg} resulting in low temperature values) and/or uncertainties in Fe^{3+}/Fe ratios.

Most of the calculated pressure values ($P_{\text{Al-in-opxBK90}}$) are in the range 5.0–5.8 GPa (at an assumed temperature of 800 °C); although for some orthopyroxene analyses with exceptionally low apparent Al contents, values up to ~8 GPa were obtained. The strong temperature dependence of this barometer (~0.9–1.0 GPa per 100 °C; Brey & Köhler, 1990) and the lack of a detectable majorite component provide additional constraints on temperature and pressure values. Therefore, we conclude that the investigated peridotites were metamorphosed under peak *P–T* conditions of ~5 GPa/800 °C.

DISCUSSION

As outlined above, the Zhimafang ultramafic massif consists of interlayered Grt- and Gf-peridotite, all of which are depleted mantle rocks with bulk-rock $Mg^{\#}$ of 0.90–0.93. The rocks show no evidence of progressive metamorphism even though calculated *P–T* conditions suggest that they reached pressures of ~5 GPa. In this section we discuss the two fundamental questions raised at the beginning of this paper: (i) where did this ultramafic massif originally come from? And (ii) are there any genetic relationships between the Zhimafang ultramafic massif and the Mesozoic subduction event between the Yangtze and North China blocks?

The origin of the Zhimafang ultramafic body

As mentioned above, Grt-peridotite has notably higher contents of Al_2O_3 and CaO, and lower MgO than GF-peridotite but both have very similar slightly LREE-enriched patterns. There are 19 intercalated layers of Grt-peridotite and GF-peridotite with regular variations in chemical composition and mineral assemblages in the core. Therefore, it is unlikely that the intercalation of the two rock types was due to pressure variations; the intercalation of these two types of peridotite is probably a result of a process other than UHP metamorphism.

Experimental data show that at high temperatures Al_2O_3 will remain in orthopyroxene, but as the temperature decreases, it is exsolved in the form of garnet and clinopyroxene. Such exsolution of clinopyroxene and garnet from orthopyroxene has been demonstrated for high-temperature harzburgites of South Africa (Cox *et al*., 1987) and of other orogenic belts (Obata & Morten, 1987). Because the granular garnet in our samples is usually spatially associated with enstatite, the very low Al_2O_3 and CaO contents and high enstatite of orthopyroxene in the Zhimafang peridotite probably reflect exsolution of garnet from a previous high-temperature orthopyroxene, which could have originated in the region of the dry peridotite solidus, roughly in the pressure range 4–8 GPa (Yamada & Takahashi, 1984). The high-temperature region near, or on, the dry peridotite solidus is favoured as the *P–T* field of origin for harzburgite precursors to garnet lherzolite, and is regarded as the region in which the pressure values of the harzburgite are broadly compatible with those of subsequent garnet lherzolite equilibration (Cox *et al*., 1987). Recrystallization, metamorphism and deformation may have obliterated such exsolution textures; however, both the mineral and rock compositions of the Zhimafang peridotite suggest that it was originally composed of harzburgite-type depleted mantle, i.e. orthopyroxene and olivine were the only original minerals in the rock Table 5.

Based on the bulk-rock MgO–FeO compositions (anhydrous basis and FeO as total Fe) (Boyd *et al*.,

Table 5. Weight percent compositions of theoretical orthopyroxene

	OPX (average of 22 analyses)	GRT (average of 42 analyses)	n1(OPX)/n2(GRT)	
wt%	n1	n2	6.00	7.00
SiO_2	58.10	41.48	55.62	55.92
Al_2O_3	0.12	21.95	3.23	2.84
TiO_2	0.01	0.03	0.02	0.02
Cr_2O_3	0.06	2.43	0.40	0.36
FeO	5.39	10.07	6.04	5.96
MnO	0.09	0.41	0.14	0.13
MgO	36.37	18.66	33.77	34.09
CaO	0.07	4.86	0.75	0.67
Na_2O	0.02	0.02	0.02	0.02
K_2O	0.01	0.01	0.01	0.01
Total	100.23	99.92	100.00	100
	Numbers of ions on the basis of 6 O	On the basis of 24 O	On the basis of 6 O	
Si	1.987	5.979	1.920	1.93
$^{(4)}Al$	0.013	0.021	0.080	0.07
$^{(6)}Al$	(0.008)	3.708	0.052	0.04
Ti	0.000	0.003	0.000	0.00
Cr	0.002	0.277	0.011	0.01
Fe^{2+}	0.154	1.214	0.174	0.17
Mn^{2+}	0.003	0.050	0.004	0.00
Mg	1.855	4.010	1.738	1.75
Ca	0.002	0.750	0.028	0.02
Na	0.001	0.005	0.001	0.00
K	0.000	0.001	0.000	0.00
Total	4.010	16.018	4.009	4.01

Total Fe as FeO.
Block number 6 means 6 portions of Opx and one portion of garnet to form 7 theoretical Opx, i.e., n1(Opx)/n2(GRT)=6.

© 2007 Blackwell Publishing Ltd

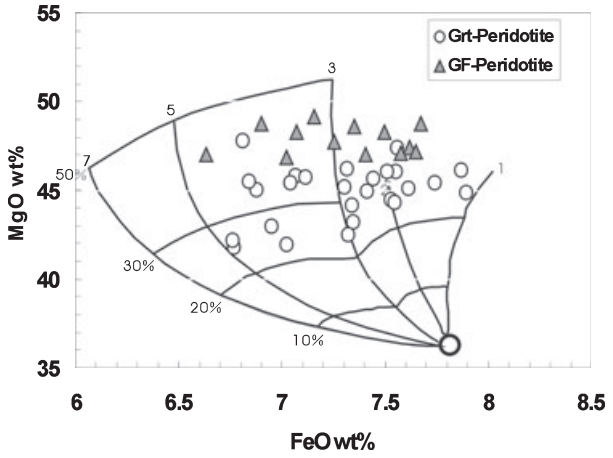


Fig. 9. Bulk-rock MgO-FeO relations for the Zhimafang peridotite (after Boyd *et al*., 2004). The melting grid outlines the expected composition of melt residues and is divided for percentage melt extracted (in 10% intervals) at different melting pressures (from 1 to 7 GPa; Walter, 1998).

2004), the Zhimafang Grt-peridotite probably underwent 20–30% partial melting, whereas the GF-peridotite may have undergone as much 35–40% partial melting (Fig. 9). This suggests that the two rock types may owe their differences to different degrees of partial melting. It is noted that both Grt-peridotite and GF-peridotite have a similar range of melting pressure (or depth) over 5 GPa, which is comparable with the 5–7 GPa peak UHP metamorphic *P–T* conditions calculated from the equilibrium mineral assemblages (Zhang *et al*., 2000) and this study. However, as no direct evidence of UHP metamorphism has been found in these rocks, this pressure can probably be regarded as the depth recorded by the rocks, and not necessarily the peak UHP metamorphic *P–T* conditions.

If it is assumed that all the garnet in these rocks was exsolved from Opx, the theoretical original orthopyroxene compositions (Table 4) can be calculated. An average of 22 Opx and 42 garnet analyses in the Grt-peridotites was used to calculate theoretical orthopyroxene compositions that originated in the region of the dry peridotite solidus. In Table 4, six portions of Opx and one portion of garnet can produce the theoretical Opx compositions shown in column 3.

Relationship between the Zhimafang ultramafic body and Mesozoic subduction

Zhang R.Y. *et al*. (2005a) reported a 220-Ma U-Pb date for zircon from the Zhimafang peridotite, which they interpreted as the peak UHPM age. This age is comparable with the peak UHP metamorphic age of the Weihai peridotite based on U-Pb dates of coesite-bearing zircon (Yang *et al*., 2003). However, there are obvious differences between these two cases.

The Weihai ultramafic body recorded the UHPM event evidenced in coesite and omphacite inclusions in a metamorphic rim to zircon which was dated at 220 Ma (Yang *et al*., 2003). These rims have Th/U ratios of <0.1, suggesting that subduction-related fluids were incorporated into the rock (Katayama *et al*., 2001; Yang *et al*., 2003; Liu *et al*., 2004).

Zircon in the Zhimafang peridotite contains inclusions of olivine, Opx, Cpx, Ti-Chu and apatite, the same mineral assemblage as that in the peridotite. This zircon also has high Th/U ratios between 0.2 and 0.8, a feature that is rare in metamorphic zircon (Katayama *et al*., 2001; Liu *et al*., 2004), but which can be probably inherited from earlier grains. This interpretation is supported by the Hf isotope compositions of zircon from the Zhimafang peridotite, which indicate that the protolith of the garnet peridotite was at least Mesoproterozoic in age (TDM model ages of 1.4 Ga) (Zheng *et al*., 2006). The Os isotopes of the peridotites, also point to an ancient (>1 Ga) mantle. The isotopic character of these rocks suggests that they represent a fragment of a continental mantle wedge rather than mantle associated with subducting oceanic lithosphere. (E. Widom, pers. comm.).

On the other hand, oxygen isotope data for the minerals from both the Grt-peridotite and GF-peridotite also confirm that the Zhimafang ultramafic body is a mantle block without crustal contamination (Zhang *et al*., 2005a,b). Fifteen spot analyses, including separated garnet, Opx, Cpx and olivine, have an average value of 5.75‰ in $\delta^{18}O$‰ with a standard deviation of 0.3‰. These values are indistinguishable from those of mantle nodules and megacrysts, suggesting that the garnet peridotite may have originated from an enriched mantle source in the sub-cratonic lithosphere, isolated from mantle convection.

Zhang *et al*. (2005a,b) suggested that the 220-Ma age of zircon in the Zhimafang ultramafic body represents the regional UHPM event. However, an alternative interpretation is that this date is the age of rocks directly exhumed from the deep mantle in a subduction–collision environment. In this case, the zircon would be ancient inherited grains modified by mantle fluids (Zhang *et al*., 2007) rather than by crustal fluids related to subduction.

CONCLUSIONS

The Zhimafang ultramafic body in the Sulu UHPM belt is a highly depleted mantle peridotite, composed of alternating layers of Grt- and GF-peridotite. The alternating layers probably reflect variations in partial melting in the Mesoproterozic other than pressure variations during metamorphism. The 220-Ma U-Pb age recorded in zircon from the peridotites is similar to the collision age between the Yangtze and North China blocks, and has been regarded as the UHPM age of the rocks (Zhang *et al*., 2005a,b). However, no evidence was found of UHP metamorphism in these rocks, In-

© 2007 Blackwell Publishing Ltd

stead, the oxygen isotopic compositions of the rocks (Zhang Z. *et al*., 2005b), their mineral and isotopic character (Zhang *et al*., 2007), the Lu-Hf and U-Pb isotopes of the zircon (Zheng *et al*., 2006), and the Os isotopes of the rocks (E. Widom, pers. comm.) all suggest that the body represents a mantle wedge with no evidence of crust contamination. Thus, we suggest that this block was probably derived directly from deep mantle as an exhumed slab within the subduction zone.

ACKNOWLEDGEMENTS

We thank Prof. L. Yongzeng of the Sixth Geological Team of Jiangsu province for his contribution to PP1 core-logging. Thanks also go to Prof. P. Robinson and two reviewers, Prof. R. Altherr and an anonymous reviewer, for their important comments and suggestions which have great improved the original manuscript. This research was funded by the CCSD 973 project (2003CB716500) and NSF of China (40399140), and the NSF EAR-0003355 and EAR-0506901 to R.Y.Z. and Z.G.L.

REFERENCES

Ahrens, T. J., 1989. Water storage in the mantle. *Nature*, **342,** 122–123.

Ames, L., Tilton, G. R. & Zhou, G. Z., 1993. Timing of collision of the Sino-Korean and Yangtze cratons. *Geology*, **21,** 339–342.

Boyd, F. R., 1989. Compositional distinction between oceanic and cratonic lithosphere. *Earth and Planetary Science Letters*, **96,** 15–26.

Boyd, F. R., Person, D. G., Hoal, K. O. *et al*., 2004. Garnet lherzolites from Louwrensia, Namibia: bulk composition and P/T relations. *Lithos*, **77,** 573–592.

Brey, G. P. & Köhler, T., 1990. Geothermobarometry in four-phase lherzolites II. New thermobarometers, and practical assessment of existing thermobarometers. *Journal of Petrology*, **31,** 1352–1378.

Brey, G. P., Doroshev, A. M., Girnis, A. V. & Turkin, A. I., 1999. Garnet-spinel-olivine-orthopyroxene equilibria in the FeO-MgO-Al_2O_3-SiO_2-Cr_2O_3 system: I. Composition and molar volumes of minerals. *European Journal of Mineralogy*, **11,** 599–617.

Canil, D. & O'Neill, H. St C., 1996. Distribution of ferric iron in some upper-mantle assemblages. *Journal of Petrology*, **37,** 609–635.

Cong, B. L., Zhang, R. Y., Li, S. & Zhai, M., 1992. Preliminary study of isotope chronology of ecologites in northern Jiansu and eastern Shangdong Provinces, China. In: *Exploration of Volcanoes and Rocks in Japan, China and America: Commemorative Papers for Prof. Yukio Matsunoto*, pp. 411–417. Yamaguchi University, Yamaguchi.

Cox, K. G., Smith, M. R. & Beswetherick, S., 1987. Textural studies of garnet lherzolites: evidence of exsolution origin from high-temperature harzburgites. In: *Mantle Xenoliths* (eds Nixon, P. H.), pp. 537–550. Wiley, Chichester, UK.

Girnis, A. V. A. B. & Brey, G. P. A., 1999. Garnet-spinel-olivine-orthopyroxene equilibria in the FeO-MgO-Al_2O_3-SiO_2-Cr_2O_3 system: II. Thermodynamic analysis. *European Journal of Mineralogy*, **11,** 619–636.

Hacker, B. & Wang, Q. C., 1995. Thermal history of ultrahigh-pressure rocks, Dabie Mountains, China. *Tectonics*, **14,** 994–1006.

Hirajima, T., Ishiwatari, A., Cong, B. L., Zhang, R. Y., Banno, S. & Nozaka, T., 1990. Identification of coesite in Mengzhong eclogite from Donghai county, northeastern Jiangsu Province, China. *Mineralogical Magazine*, **54,** 579–584.

Irifune, T., 1987. An experimental investigation of the pyroxene-garnet transformation in a pyrolite composition and its bearing on the constitution of mantle. *Physics of the Earth and Planetary Interiors*, **45,** 324–326.

Jahn, B. M., 1998. Geochemical and isotopic characteristics of UHP eclogites and ultramafic rocks of the Dabie orogen. Implications for continental subduction and collision tectonics. In: *When Continents Collide. Geodynamics and Geochemistry of Ultrahigh-Pressure Rocks* (eds Hacker, B. & Liou, J. G.), pp. 203–239. Dordrecht, Kluwer.

Katayama, I., Maruyama, S., Parkinson, C. T., Terada, K. & Sano, Y., 2001. Iron micro-probe U-Pb zircon geochronology of peak and retrograde stages of ultrahigh-pressure metamorphic rocks from the Kokchetav massif, northern Kazakhstan. *Earth and Planetary Science letters*, **188,** 185–198.

Kretz, R., 1983. Symbols for rock-forming minerals. *American Mineralogist*, **68,** 277–279.

Krogh, E. J., 1988. The garnet-clinopyroxene Fe-Mg geothermometer-reinterpretation of existing experimental data. *Contributions to Mineralogy and Petrology*, **99,** 44–48.

Krogh Ravna, E. J. & Paquin, J., 2003. Thermobarometric methodologies applicable to eclogites and garnet ultrabasites. In: *Ultra-high Pressure Metamorphism, EMU Notes in Mineralogy 5* (eds Carswell, D. A. & Compagnoni, R.), pp. 229–259. Eötvös University Press, Budapest.

Li, S. G., Chen, Y., Cong, B. L. *et al*., 1993. Collision of the North China and Yangtze blocks and formation of coesite-bearing eclogite: timing and processes. *Chemical Geology*, **109,** 70–89.

Liou, J. G. & Zhang, R. Y., 1998. Petrogenesis of an ultrahigh-pressure garnet-bearing ultramafic body from Maowu, Dabie Mountains, east-central China. *The Island Arc*, **7,** 115–134.

Liu, F. L., Xu, Z. Q., Liou, Z. G. *et al*., 2002. Ultrahigh-pressure mineral inclusions in zircons from gneissic core samples of the Chinese continental scientific drilling site in eastern China. *European Journal of Mineralogy*, **14,** 499–512.

Liu, F. L., Xu, Z. Q., Liou, Z. G. & Song, B., 2004. SHRIMP U-Pb ages of ultrahigh-pressure and retrograde metamorphism of gneisses, south-western Sulu terrane, eastern China. *Journal of Metamorphic Geology*, **22,** 315–326.

Luth, R. W. & Canil, D., 1993. Ferric iron in mantle-derived pyroxenes and a new oxybarometer for the mantle. *Contributions to Mineralogy and Petrology*, **113,** 236–248.

Luth, R. W., Virgo, D., Boyd, F. R. & Wood, B. J., 1990. Ferric iron in mantle-derived garnets. *Contribution to Mineralogy and Petrology*, **104,** 56–72.

O'Neill, H. St. C. & Wood, B. J., 1979. An experimental study of Fe-Mg partitioning between garnet and olivine and its application as a geothermometer. *Contributions to Mineralogy and Petrology*, **70,** 59–70.

O'Neill, H. St C. & Wood, B. J., 1980. An experimental study of Fe-Mg partitioning between garnet and olivine and its calibration as a geothermometer: corrections. *Contributions to Mineralogy and Petrology*, **72,** 337.

Obata, M. & Morten, L., 1987. Transformation of spinel lherzolite to garnet lherzolite in ultramafic lenses of the Austridic Crystalline Complex, Northern Italy. *Journal of Petrology*, **28,** 599–632.

Okay, A. T. & Sengor, A. M. C., 1992. Evidence for intra-continental thrust related exhumation of the ultra-high pressure rocks in China. *Geology*, **20,** 411–414.

Okay, A. I., Xu, S. & Sengör, A. M. C., 1989. Coesite from the Dabie Shan eclogites, central China. *European Journal of Mineralogy*, **1,** 595–598.

Rumble, D. & Yui, T. F., 1998. The Qinglongshan oxygen and hydrogen isotope anomaly near Donghai in Jiangsu province, China. *Geochemica et Cosmochemica Acta*, **62,** 3307–3321.

© 2007 Blackwell Publishing Ltd

Schumacher, J. C., 1991. Empirical ferric iron corrections: necessity, assumptions and effects on selected geothermobarometers. *Mineralogical Magazine*, **55,** 3–18.

Smith, D., 1999. Temperatures and pressures of mineral equilibration in peridotite xenoliths: review, discussion, and implications. In: *Mantle Petrology: Field Observations and High-Pressure Experimentation. A Tribute to Francis R. (Joe) Boyd, Special Publication 6* (eds Fei, Y., Bertka, C. M. & Mysen, B. O.), pp. 171–188. Geochemical Society, Special publications, Houston, TX.

Streckeisen, A., 1976. To each plutonic rock its proper name. *Earth Sciences*, **12,** 1–33.

Walter, M. J., 1998. Melting of garnet peridotite and the origin of kimberlite and depleted lithosphere. *Journal of Petrology*, **39,** 29–60.

Wang, X. M. & Liou, J. G., 1991. Regional ultrahigh-pressure coesite-bearing eclogitic terrane in central China: evidence from country rocks, gneiss, marble, and metapelite. *Geology*, **19,** 933–936.

Wang, X. M., Liou, J. G. & Mao, H. K., 1989. Coesite-bearing eclogites from the Dabie Mountains in central China. *Geology*, **17,** 1085–1088.

Xu, Z. Q., 1987. *Etude tectonique et microtectonique de la China Paleozoique et Triasique des Qinlings (China)*. Thesis de doctorate, Univ Sci Tech Languedoc, Montpellier.

Xu, Z. Q., Yang, W. C., Zhang, Z. M. & Yang, T. N., 1998. Scientific significance and site-selection researches of the first Chinese continental scientific deep drillhole. *Continental Dynamics*, **3,** 1–13.

Xu, Z. Q., Chen, J., Yang, J. S., Li, P. & Chen, F. Y., 2003. Discovery of titanoclinohumite and titanochondrodite exsolution in clinopyroxene included in garnet peridotite and their significance. *Acta Geologica Sinica*, **77,** 547–555.

Xu, S. T., Liu, y. C., Chen, G. B., Ji, S. Y., Ni, P. & Xiao, W. S., 2005. Microdiamonds, their classifications for the host eclogites from the Dabie and Su-Lu regions in central eastern China. *Mineralogical Magazine*, **69,** 509–520.

Yamada, H. & Takahashi, E., 1984. Subsolidus phase relations between coexisting garnet and two pyroxenes at 50 to100 kbar in the system CaO-MgO-Al_2O_2-SiO_2. In: *Kimberlites, I. II. The mantle and crust-mantle relationships* (ed. Kornprobst, Q. V.), pp. 247–255. Elsevier, Amsterdam.

Yang, J. J., 1991. *Eclogites, Garnet, Pyroxenites and Related Ultrabasics in Shangdong and North Jiangsu of East China*. Geological Publishing House, Beijing (in Chinese).

Yang, J. S., Xu, Z. Q. & Bai, W. J., 1999. The discovery of diamond in the eclogite from the Sulu region. *Earth Science Frontier*, **6,** 69. (in Chinese).

Yang, J. S., Wooden, J. L., Wu, C. L. *et al*., 2003. SHRIMP U-Pb dating of coesite-bearing zircons from the ultrahigh-pressure metamorphic rocks, Sulu terrane, east China. *Journal of Metamorphic Geology*, **21,** 551–560.

Zhang, R. Y. & Liou, J. G., 1994. Significance of magnesite paragenesis in ultrahigh-P metamorphic rocks. *American Mineralogist*, **79,** 397–400.

Zhang, R. Y., Liou, J. G. & Cong, B. L., 1994. Petrogenesis of garnet-bearing ultramafic rocks and associated eclogites in the Su-Lu ultrahigh-P metamorphic terrane, eastern China. *Journal of Metamorphic Geology*, **12,** 169–186.

Zhang, R. Y., Liou, J. G., Yang, J. S. & Yui, T. F., 2000. Petrochemical constraints for dual origin of garnet peridotites from the Dabie-Sulu UHP terrane, eastern-central China. *Journal of Metamorphic Geology*, **18,** 149–166.

Zhang, R. Y., Yang, J. S., Wooden, J. L., Liou, J. G. & Li, T. F., 2005a. U-Pb SHRIMP geochronology of zircon in garnet peridotite from the Sulu UHP terrane, China: Implications for mantle metasomatism and subduction-zone UHP metamorphism. *Earth and Planetary Science Letters*, **237,** 729–743.

Zhang, Z. M., Rumble, D., Liou, J. G., Xiao, Y. L. & Gao, Y. J., 2005b. Oxygen isotope geochemistry of rocks from the Pre-Pilot Hole of the Chinese Continental Scientific Drilling Project (CCSD-PPH1). *American Mineralogist*, **90,** 857–863.

Zhang, R. Y., Li, T., Rumble, D., Yui, T.-F., Li, L., Yang, J. S., Pan, Y. & Liou, J. G., 2007. Multiple metasomatism in Sulu ultrahigh-P garnet peridotite constrained by petrological and geochemical investigations. *Journal of Metamorphic Geology* doi:10.1111/j.1525–1314.2006.00683.x.

Zheng, J., Grigffin, W. L., O'Reily, S. Y., Yang, J. S. & Zhang, R. Y., 2006. A refractory mantle protolith in younger continental crust, east-central China: Age and composition of zircon in the Sulu ultrahigh-pressure peridotite. *Geology*, **34,** 705–708.

Received 25 April 2006; revision accepted 11 October 2006.

© 2007 Blackwell Publishing Ltd